Bedrock depth influences spatial patterns of summer baseflow, temperature, and flow disconnection for mountainous headwater streams

Martin A. Briggs[1*]

Phillip Goodling[2]

Zachary C. Johnson[3]

Karli M. Rogers[4]

Nathaniel P. Hitt[4]

Jennifer B. Fair[4,5]

Craig D. Snyder[4]

[1]U.S. Geological Survey, Earth System Processes Division, Hydrogeophysics Branch, 11 Sherman Place, Unit 5015, Storrs, CT 06269 USA
[2]U.S. Geological Survey, Maryland-Delaware-District of Colombia Water Science Center, 5522 Research Park Drive, Catonsville, MD, 21228, USA
[3]U.S. Geological Survey, Washington Water Science Center, 934 Broadway, Suite 300, Tacoma, WA 98402 USA
[4]U.S. Geological Survey, Eastern Ecological Science Center, 11649 Leetown Road, Kearneysville, WV 25430 USA
[5]U.S. Geological Survey, New England Water Science Center, 10 Bearfoot Road, Northborough, MA 01532 USA

Corresponding author: Martin Briggs, mbriggs@usgs.gov

Abstract

In mountain headwater streams the quality and resilience of cold-water habitat is regulated by surface streamflow connectivity and groundwater exchange. These critical hydrologic processes are thought to be influenced by the stream corridor bedrock contact depth (sediment thickness), which is often inferred from sparse hillslope borehole information, piezometer refusal, and remotely sensed data. To investigate how local bedrock depth might control summer stream temperature and channel disconnection (dewatering) patterns, we measured stream corridor bedrock depth by collecting and interpreting 191 passive seismic datasets along eight headwater streams in Shenandoah National Park (Virginia USA). In addition, we used multi-year stream temperature and streamflow records to calculate summer baseflow metrics along and among the study streams. Finally, comprehensive visual surveys of stream channel dewatering were conducted in 2016, 2019, and 2021 during summer baseflow conditions (124 total km of stream length). We found that measured bedrock depths were not well-characterized by soils maps or an existing global-scale geologic dataset, where the latter overpredicted measured depths by 12.2 m (mean), or approximately four times the average bedrock depth of 2.9 m. Half of the eight study stream corridors had an average bedrock depth of less than 2 m. Of the eight study streams, Staunton River had the deepest average bedrock depth (3.4 m), the coldest summer temperature profiles, and substantially higher summer baseflow indices compared to the other study steams. Staunton River also exhibited paired air and water annual temperature signals suggesting deeper groundwater influence, and the stream channel did not dewater in lower sections during any baseflow survey. In contrast, Paine Run and Piney River did show pronounced, patchy channel dewatering, with Paine Run having dozens of discrete dry channel sections ranging 1 to greater than 300 m in length. Stream dewatering patterns were apparently influenced by a combination

of discrete deep bedrock (20+ m) features and more subtle sediment thickness variation (1-4 m), depending on local stream valley hydrogeology. In combination these unique datasets show the first large-scale empirical support for existing conceptual models of headwater stream disconnection based on underflow capacity and shallow groundwater supply.

1. Introduction

Mountain headwater stream habitat is influenced by hydrologic connectivity along the surface channel, and connectivity between the channel and multiscale groundwater flowpaths (Covino, 2017; Fausch et al., 2002; Wohl, 2017). Discharge from shallow groundwater within the critical zone is a primary component of stream baseflow, attenuating maximum summer temperatures and creating cold water habitat (Singha and Navarre-Sitchler, 2021; Sullivan et al., 2021) and shaping catchment topography (Litwin et al., 2022). In headwater stream valleys characterized by irregular bedrock topography and thin, permeable sediments, nested physical processes interact to control the connectivity of groundwater/surface water exchange (Tonina and Buffington, 2009). Between stormflow and snowmelt events, headwater streamflow (baseflow) is primarily generated by groundwater discharge due to a relative lack of soil water storage and release (Winter et al., 1998). Unlike in lower valley settings, mountain headwaters accumulate less fine soil, facilitating efficient routing of quickflow to streams through macropores and other preferential flowpaths within regolith and saprolite (Sidle et al., 2000). Recharge that does percolate vertically contributes to shallow groundwater along steep hillslopes and valley floors, where groundwater flowpath depths are constrained by bedrock topography (Buttle et al., 2004). Although deeper groundwater may also represent an important contribution to summer streamflow in systems with relatively permeable bedrock (Burns et al., 1998; O'Sullivan et al., 2020), shallow, low permeability bedrock generally restricts stream-groundwater connectivity to the thin layers of unconsolidated sediments (Briggs et al., 2018b).

In addition to baseflow drainage along headwater stream networks, down-valley shallow groundwater 'underflow' can be substantial when high gradient streams lack sinuosity and flow over permeable sediment (Figure 1a, Figure A1). In fact, headwater stream channels may only be expected to show surface flow when the transmission ability of the underlying alluvium and colluvium is exceeded, and bedrock depth is thought to be a primary control of this underflow capacity (Ward et al., 2020). In some hydrogeologic settings, underflow can dominate groundwater export from mountain catchments compared to groundwater drainage via the surficial stream channel (Larkin and Sharp, 1992; Tiwari et al., 2017). Moreover, in addition to longitudinal transport down-valley, underflow also acts as a reservoir of exchange for hyporheic flowpaths that may mix with shallow groundwater before returning to channel flow (Payn et al., 2009), transporting buffered temperature signals back to channel waters (Wu et al., 2020). Local underflow is recharged from upgradient flowpaths and adjacent hillslopes, creating complex seasonal and interannual patterns in groundwater connectivity and discharge to surface water (Jencso et al., 2010; Johnson et al., 2017). A major challenge to understanding groundwater exchange in headwaters is that attributes of the streambed subsurface, such as the depth to the underlying bedrock contact, are often only available from limited direct measurements, coarse spatial interpolations, or inferred remotely based on landscape forms. Therefore, methods that allow efficient, local measurements of the streambed subsurface are critically needed.

Seasonal thermal regimes of mountain headwater streams can be profoundly impacted by groundwater inflow from multiple depths (Briggs et al 2018a). In lower valley settings, the temperature of groundwater discharge along stream networks is often assumed to be constant throughout the year and approximate the average annual land surface temperature (Stonestrom and Constantz, 2003). Conversely, shallow groundwater temperature (within several m from land surface) can show pronounced seasonality (Bundschuh, 1993; Lapham, 1989) and high spatial variability, even over small spatial extents (Snyder et al. 2015). The warming of shallow groundwater during the summer and fall seasons can limit the ability of gaining mountain streams to support cold-water fish populations during the low flow season, even if baseflow (assumed to be dominated by groundwater discharge) fractions are large (Johnson et al., 2020). In systems with low permeability bedrock, thicker hillslope sediments may generate deeper, colder lateral groundwater flow to streams in summer (Figure 1a), increasing cold water habitat resiliency (Briggs et al., 2018b). For example, a recent meta-analysis of stream and air temperature records across the contiguous United States found that a substantial fraction of shallow groundwater dominated streams displayed summer warming trends in recent decades, while deeper groundwater dominated streams were more stable (Hare et al., 2021). Steep mountain stream systems such as those found in the Blue Ridge and Cascade mountains of the USA have been found to show annual thermal regimes dominated by the annual thermal signals indicative of shallow groundwater (Johnson et al., 2020), indicating such streams may also be at risk for warming over time, contrary to assumptions based on elevation alone.

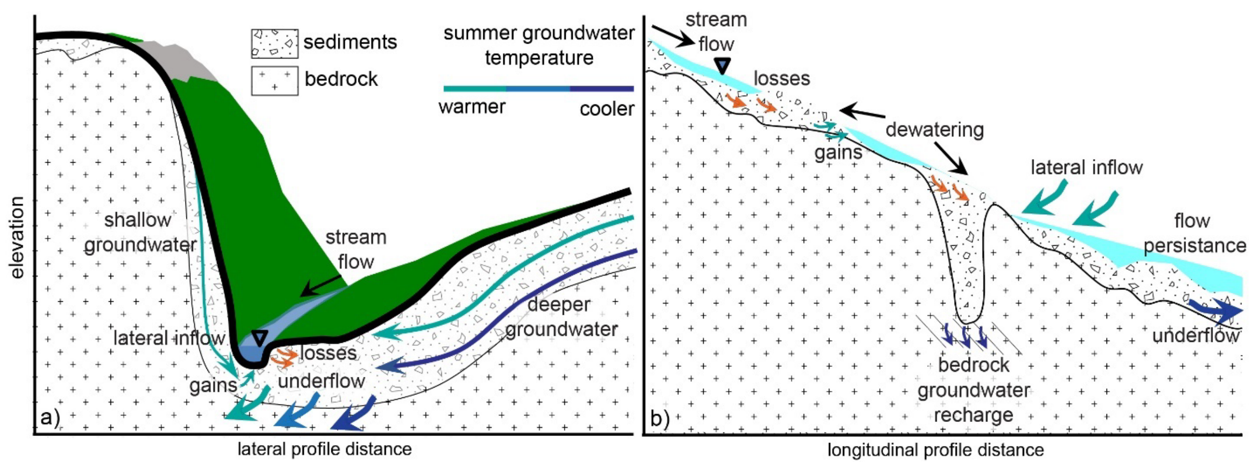

Figure 1. A conceptual mountain stream valley cross section (panel a) and longitudinal profile (panel b) indicating the expected control of low permeability bedrock topography on groundwater temperature, stream-groundwater exchange, patchy stream dewatering, and the underflow reservoir.

Beyond warm summer stream temperatures, the dewatering and disconnection of the active stream channel during summer low flows can adversely impact fish habitat by impeding fish movement (Edge et al., 2017; Labbe & Fausch, 2000; Rolls et al., 2012; Snyder et al., 2013), locally degrading water quality (Hopper et al., 2020), and increasing predation risks in isolated pools (Magoulick and Kobza 2003). However, the physical controls on localized stream channel dewatering are not well characterized and likely involve a spectrum of nested gaining and losing flowpaths. For mountain headwater streams, previous research has documented major contractions of drainage networks during seasonal drydown (Ilja Van Meerveld et al., 2019) and general seasonal shifts in hydraulic gradients from gaining to losing, with closely coupled streamflow and precipitation events, indicating a dominance of shallow routing rather than deeper groundwater connectivity in maintaining streamflow (Zimmer and McGlynn, 2017). Warix et a l., (2021) found that although deeper/older groundwater was found to contribute to their study streams during dry down, those sources were insufficient in preventing dry channel sections from occurring, also indicating the importance of shallow groundwater inflows and local geologic controls. Locally-losing sections of headwater stream channels can be associated with coarse, permeable colluvial deposits from hillslope mass wasting processes (Costigan et al., 2016; Weekes et al., 2015), as local enhancement of the total pore space under mountain streams can drive downwelling of streamwater (Figure 1b, Tonina & Buffington, 2009). Main channel dewatering occurs when the bed sediments have a storage and transport capacity that exceeds stream discharge (Rolls et al., 2012; Ward et al., 2018), though stream water losses can also be driven by local changes in bed morphology and slope (Costigan et al., 2016) and bedrock permeability. The shallowing of the underlying bedrock contact may drive lateral underflow toward the surface causing the channel to gain water (Herzog et al., 2019, Figure 1b), though such hypothesized dynamics are not well documented in existing literature due to a relative lack of bedrock topography data along headwater streams.

At large scales, contiguous bedrock depth layers are interpolated from a combination of relatively sparse borehole data and surface topography (Kauffman et al., 2018; Pelletier et al., 2016; Shangguan et al., 2017). However, in steep headwater systems with little borehole data, bedrock topography is difficult to predict accurately from land surface topography alone. The development of improved tools for predicting bedrock depth is an active area of research which has recently demonstrated promise when bedrock outcrop data are included (e.g. Furze et al., 2021; Odom et al., 2021). The limitations of using landform data to predict bedrock depth are compounded by inherent challenges in collecting physical data via soil pits and monitoring wells in rugged, rocky terrain, and so direct measurement data are often limited to highly studied experimental watersheds where bedrock depth is still only *inferred* from piezometer installation refusal (e.g. Jencso et al., 2010; Ward et al., 2018). In more typical headwater systems, existing wells may be preferentially installed to maximize the production of water and not broadly sample the true range of bedrock depths.

Application of near surface geophysical methods to stream corridor research has increased appreciably in recent years (McLachlan et al., 2017), and several methods are sensitive to shallow subsurface flow and geologic attributes including bedrock depth. Active seismic refraction measurements can provide high resolution (10s of cm) bedrock depth information along transect-based cross-sections (e.g. Flinchum et al., 2018), but are less suited for exploration throughout rugged mountain stream valleys at the many km-scale due to logistical challenges in using active seismic methods to obtain a sufficient amount of data to effectively characterize important variation in bedrock depth at relatively small, ecologically-relevant spatial scales.

Point-based, efficient passive seismic measurements represent a unique combination of high mobility and relative precision for measuring bedrock depth along mountain valleys. The horizontal-to-vertical spectral ratio (HVSR) method is a passive seismic technique that evaluates ambient seismic noise recorded using handheld instruments placed on the ground surface to identify seismic resonance that develops due to strong vertical changes in subsurface acoustic impedance (Yanamaka et al., 1994). While typically insensitive to variations in unconsolidated sediment permeability (i.e., clay lenses), the HVSR method is effective at identifying the depth to distinct unconsolidated sediment/bedrock interfaces at essentially the 'point' spatial scale. HVSR measurements are often not successful in settings with highly weathered bedrock surfaces such as those with pronounced epikarst and saprolite.

The control of stream to groundwater exchange (i.e., 'transmission losses') on streamflow permanence has been highlighted as an important research need by the comprehensive review of intermittent stream systems by Costigan et al., (2016). Following the conceptual model of Ward et al., (2018) for mountain stream corridors, a central hypothesis of our research was that bedrock depth along the stream corridor will act as a first-order control on stream dewatering patterns when shallow bedrock is of low permeability. Based on the concepts presented by Tonina & Buffington, (2009), we postulated that relatively thick, permeable surficial sediment zones could locally accommodate the entirety of low streamflow volumes, dewatering main channel sections at varied scales when not balanced by groundwater inflow (Figure 1b). We further hypothesized that summer stream channel thermal regimes would also be influenced by bedrock depth, as the temperature of groundwater flowpaths that generate baseflow is depth dependent (Briggs et al., 2018b), indicated conceptually in Figure 1a. To test our hypotheses, we extended the existing mountain headwater bedrock depth surveys from Shenandoah National Park (SNP), Virginia, USA (citation) to seven additional subwatersheds and compared results to physical mapping of stream dewatering, multi-year stream temperature data and derived groundwater influence metrics, and baseflow separation analysis to address the following research questions:

1. Does stream corridor bedrock depth exhibit longitudinal spatial structure in mountainous streams at ecologically relevant spatial scales? Can measured bedrock depth dynamics be accurately extracted from existing large-scale datasets or inferred from high resolution soils maps?

2. Does underflow generally represent a net source or sink of summer flow for headwater streams based on observed dewatering patterns and groundwater influence metrics?

3. Does bedrock depth explain spatial variation in stream temperature and summer baseflow indices within headwater streams?

2. Study Area

SNP is an 800 km^2 area of preserved headwater forest perched along a major ridgeline of the Blue Ridge Mountains in northern VA, USA (Figure 2). The bedrock of the park is predominantly low permeability basaltic and granitic material in the central and northern sections, and siliciclastic along the southern section (Southworth et al., 2009), though many subwatersheds also transition in dominant bedrock type from high to lower elevation. Stream valleys of SNP are typically steep and feature a perennial channel with mainly non-perennial tributaries (Johnson et al., 2017, Figure A1) and stream baseflow consists of less than 3-yr old groundwater on average (Plummer et al., 2001). In contrast, water collected from SNP hillslope wells completed in shallow fractured rock generally have higher ages of 10-20 yr (Plummer et al., 2001), indicating minimal contributions from bedrock groundwater to streamflow. Previous ecohydrological research in SNP has noted that some mainstem stream channels show patchy dewatering at summer low flows (Snyder et al., 2013), though the physical controls on these patterns of stream drying were not clear.

In SNP, stream baseflow is thought to be predominantly generated by near-surface drainage of coarse unconsolidated alluvium and colluvium (DeKay, 1972; Nelms and Moberg, 2010). The mountain ridgeline streamflow systems are expected to drain near-surface flowpaths and accommodate substantial down valley underflow below perennial stream channels (Figure A1). A portion of hillslope recharge is expected to percolate downward through connected bedrock fractures into the deeper groundwater reservoir contributing to mountain block recharge along the Shenandoah River Valley. Narrow alluvium deposits mapped along the stream corridors of SNP are thought to generally range up to 6 m in thickness and be more clay rich when sourced by basaltic bedrock (Southworth et al., 2009). Data at sparse wells drilled along the SNP ridgeline indicate bedrock depth can range over 20 m on hillslopes and be highly variable (DeKay, 1972; Goodling et al., 2020; Lynch, 1987).

Previous research has inferred summer and annual groundwater discharge patterns throughout SNP subwatersheds based on paired, local air and stream water temperature dynamics (Briggs et al., 2018a; Johnson et al., 2017; Snyder et al., 2015). Combined, these analyses indicated groundwater exchange is highly variable in space along singular stream valleys and between subwatersheds, and dependent upon local- to subwatershed-scale characteristics. A combination of landform features that include stream slope and stream valley confinement operate in conjunction with seasonal precipitation to drive groundwater influence on summer stream temperatures (Johnson et al., 2017). Multi-week lags in time between streamwater and local air annual temperature signals (i.e., water phase shifts toward later time) were observed from dozens of the 120 total monitored stream sites indicating a dominance of shallow groundwater discharge, originating generally within approximately 3 m of land surface (Briggs et al., 2018a).

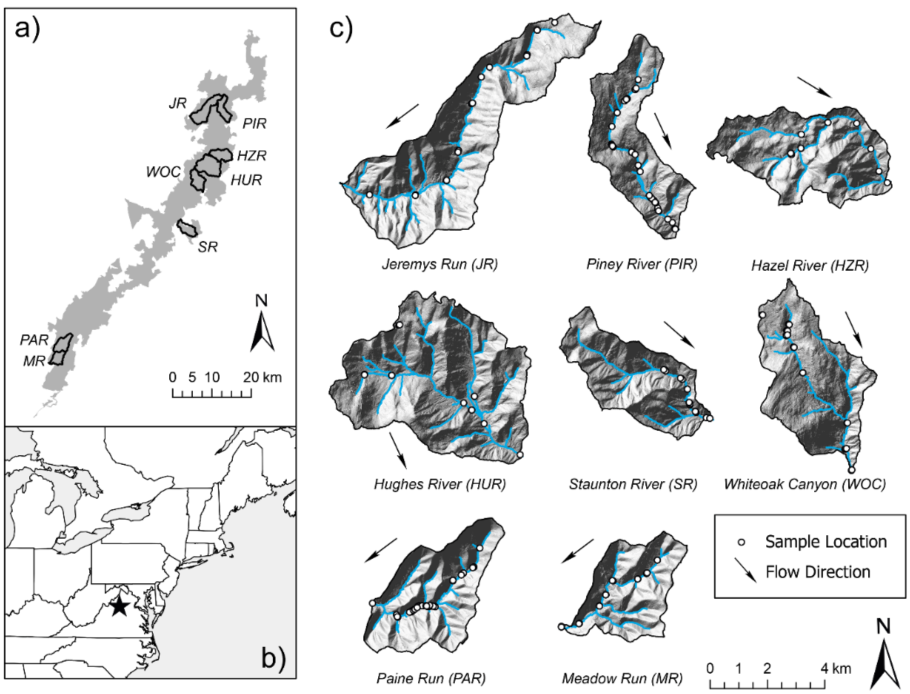

Figure 2. This study was based in Shenandoah National Park (panel a) located in the Blue Ridge Mountains of northeast USA (panel b). LiDAR hillshade cutouts of each subwatershed illustrate the rugged terrain and varied valley morphology (panel c). The mainstem stream channel and tributaries are traced and passive seismic sample measurement locations noted.

3.0 Methods

3.1 Passive Seismic Bedrock Depth Measurements

Periodically from the summer of 2016 to the spring of 2020, we acquired 323 HVSR measurements across SNP. The geophysical data were collected along the perennial streams of seven subwatersheds with extensive existing stream temperature and ecological datasets, and at known ridgeline and hillslope borehole locations. This effort added to previously interpreted HVSR data from 22 riparian sites collected along the Whiteoak Canyon subwatershed in late 2015 (Briggs et al., 2017), for a total of 8 mountain streams for analysis in this study (Figure 2). In July 2016, HVSR data were collected in the following subwatersheds: Piney River, Paine Run, Meadow Run, Jeremys Run, Hazel River, and Hughes River. Some stream sections were inaccessible due to steep bedrock walls and waterfalls, resulting in poor data coverage in those areas.

Figure 3. Typical sections of a) Paine Run, b) Piney River, c) Staunton River, and d) a section of Paine Run that was dewatered at baseflow leaving isolated pools. The passive seismic HVSR instruments are shown deployed in panels a), b) and d) (Photographs by the U.S. Geological Survey).

Measurement locations mostly coincided with existing stream temperature monitoring stations (described by Snyder et al., 2017), and were typically made at points immediately adjacent to the stream or on larger rocks within the channel (Figure 3). In July 2019, HVSR data were again collected along Paine Run and Piney River subwatersheds, and throughout the lower Staunton River (Figure 3). The 2019 survey design differed in that transect measurements were made at 4 locations along the stream channel waterline spaced approximately 25 m apart at longitudinal locations that differed from the 2016 survey. This was done to assess potential variation in bedrock depth along short subreaches of these three streams. Finally, clustered HVSR data were collected in March 2020 in Paine Run and Piney River in zones previously observed to show channel disconnection and streamflow re-emergence. Measurement locations were chosen to test the hypothesis that the dewatering patterns were controlled by bedrock depth as shown conceptually in Figure 1b.

HVSR data were collected using multi-component Tromino seismometers (MOHO, S.R.L.) directly coupled to the land surface or placed on heavy metal plates where sediment was loose. Collection times ranged 10-20 min at either 128 or 256 Hz sampling rates. HVSR data collection locations were determined by a combination of internal Tromino GPS and external GPS units. HVSR measurements were processed to derive a resonant frequency using a commercially available program (GRILLA® v. 8.0 (2018); further details regarding data processing are given by Goodling et al., (2020).

Resonant frequency measurements that passed a series of quality criteria were then converted to a bedrock depth estimate following Briggs et al., (2017). This conversion necessitates a shear wave velocity estimate for the unconsolidated sediments over bedrock. HVSR data collected at six spatially distributed boreholes with documented depth to varied-type bedrock along the SNP ridgeline indicated a mean shear wave velocity of 358.7 +/- 56 m/s (Goodling et al., 2020). A similar shear wave velocity of 346 m/s was measured at two locations along the Whiteoak Canyon riparian zone spaced several km apart using active seismic methods (Briggs et al., 2018b). This agreement indicates a common shear wave velocity can be assumed for the unconsolidated material of SNP subwatersheds. For this study we used the average of these spatially distributed active and passive seismic methods at 352 m/s. The average shear wave velocity calculated in this study is comparable to the mean shear wave velocity ranges in firm soils (180 - 360 m/s) and very dense soil and soft rock (360-760 m/s), according to National Earthquake Hazards Reduction Program (NEHRP) guidelines (Building Seismic Safety Council, 1994). As an example of measurement sensitivity to the shear wave velocity parameter for shallow bedrock contacts, a velocity change in either direction by 25 m/s would generally shift the bedrock depth estimate by <0.2 m.

3.2 Observations of spatial dewatering patterns

Longitudinal (upstream to downstream) patterns of dewatering were determined in the summers of 2016, 2019, and 2021 during baseflow conditions over 124 total km of stream length for all surveys combined. In July-August of 2016 all eight subwatersheds (Figure 2) were surveyed. In September of 2019 and August 2021, dewatering surveys were repeated in three subwatersheds (Paine Run, Piney River, and Staunton River) to evaluate annual variation in dewatering patterns. Data were collected by a team of investigators walking each stream from an upstream location defined by the point along the stream draining 75-hectares (assumed capture area required to generate perennial streamflow, determined using watershed tools in ArcGIS) to the bottom of each watershed near the park boundary, and mapping transition points between three hydrologic categories: Wet, dry, or isolated pools based upon investigator observation. "Wet" segments were defined as reaches where entire channel was wet with flow between pools;

"Dry" segments were defined as reaches containing no water, or isolated pools of insufficient depth to sustain 1+ year old brook trout; and "Isolated Pools" were defined as reaches containing pools of sufficient depth to support brook trout but were hydrologically disconnected from other parts of the channel. An example of isolated pools is photographically depicted in Figure 3d. Spatial coordinates of transition points were mapped using a Trimble R2 GNSS receiver for <1-meter accuracy. Surveys for each subwatershed were completed within a single day to minimize effects of temporal variation in precipitation.

In addition to local variability in bedrock depth, spatial patterns of dewatering and stream temperature are likely to be influenced by seasonal precipitation and air temperature proximate to the period of measurement (i.e., summer conditions, 2016 and 2019). We used historical weather records (1942 – 2020) collected from the nearby Luray Weather Station located within SNP (Station No. GHCND:USC00445096) to compare weather conditions during these two study years with historical norms. Finally, 3D surface area of each subwatershed was determined from existing LiDAR data using the Add Surface Information tool in ArcGIS and mean valley bottom width was evaluated from LiDAR data using 100-m transects measured approximately 2 m above the valley floor.

3.3 Stream channel temperature data and baseflow separation

Multi-year SNP stream temperature data were collected at hourly time intervals as described by Snyder et al., (2017) using HOBO Pro V2 thermographs (+/- 0.2 °C expected accuracy). From this larger dataset, 64 main channel locations within the 8 study subwatersheds were extracted and processed for summary statistics such as the maximum and minimum of the 7-day running mean using Matlab R2019b software (Mathworks, Inc.). Only complete 7-day periods were included in the running average. Warm season data (July, August, September) were isolated and analyzed to coincide with the stream dewatering surveys and a larger body of research regarding summer cold-water brook trout habitat in SNP. We utilized stream temperature data processed to extract annual temperature signals by Briggs et al., (2018a) where dry sensor periods were identified and removed, impacting a handful of the upper stream sites. Data were visualized and downstream trends explored using Sigmaplot 14.0 software (Systat Software Inc.). Baseflow separation was conducted for the three continuously gaged streams of this study (Paine Run, Piney River, Staunton River) over summer months for the period of record (1993-2020). Following the approach of Hare et al., (2021), the daily Baseflow Index (BFI) was calculated using the USGS-R 'DVstats' package (version 0.3.4)following methods described by Barlow et al., (2014), and dividing the calculated baseflow discharge by the corresponding stream discharge, where a value of one would indicate stream discharge was entirely composed of baseflow. BFI was then averaged (mean) across each summer season, along with the mean and standard deviation of summer stream discharge.

4. Results

4.1 Stream Corridor Bedrock depth

Approximately 60% of individual HVSR measurements (191 of the 323) were of high enough quality to be interpreted for bedrock depth using objective data quality metrics reported by the GRILLA software. This ratio of interpretable to total HVSR measurements was similar to the previous 2015 Whiteoak Canyon Run study using the same instrument type (Briggs et al., 2017). For the 132 datasets that could not be interpreted, the primary reason was no identifiably resonant frequency 'peak' in the multicomponent seismic data, as described in more detail in the data release of Goodling et al., (2020). The loosely consolidated, rocky surficial soils of many SNP subwatershed riparian zones likely contributed to poor instrument coupling to the land surface, and therefore reduced measurement sensitivity/success compared to firmer soils. However, due to spatial redundancy in the measurements, the 191 locations where bedrock depth was evaluated generally covered all the intended longitudinal stream measurement locations throughout the subwatersheds.

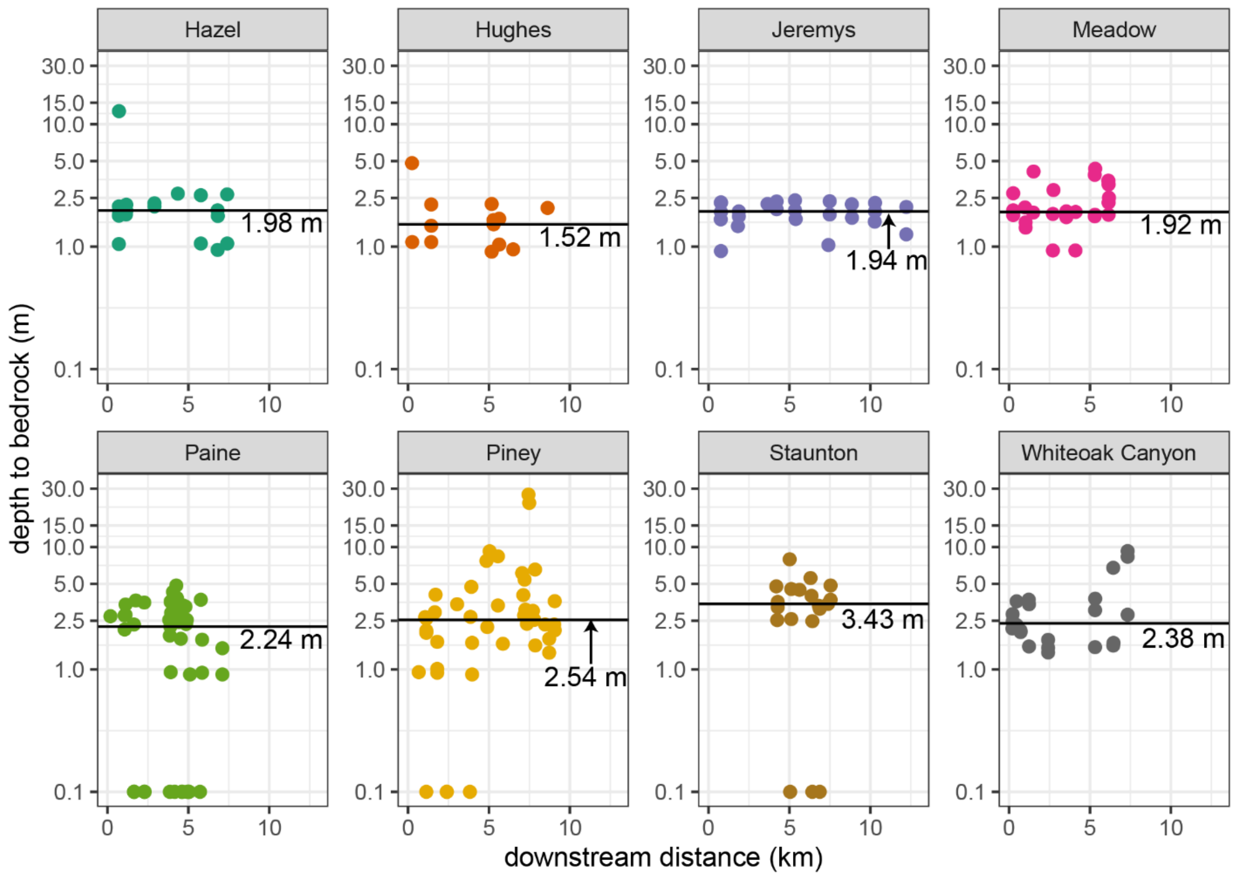

Figure 4. Measured depth to rock along the stream channel and riparian zones of the eight study subwatersheds. Exposed bedrock (i.e., zero depth) observed at the intended measurement location is noted here by a value of '0.1' on the log scale. The median value is shown as a labelled horizontal line.

The median bedrock depth was smallest for Hughes River (1.52 m), and similar for Meadow Run, Jeremys Run, Hazel River (1.92, 1.94, 1.98, respectively, Table 1, Table B1, Figure 4). Paine Run had a median of 2.24 m, Whiteoak Canyon of 2.38 m, and Piney River of

2.54 m. Lower Staunton River had the largest median depth to rock of 3.43 m (Table 1). Piney River had the largest variation in bedrock depth, including a discrete zone greater than 20 m deep, along with several zones of exposed bedrock along the channel. Visual observations of exposed channel bedrock were not incorporated into the bedrock depth averages presented in Table 1. Simple bivariate relations were explored between the physical valley parameters, and a negative relation was found between bedrock depth and mean valley bottom width while other relations were not significant.

Table 1. *The median bedrock depth along with the elevation, mean, and 7-d maximum summer temperatures over the period of record collected at most downstream site location in each subwatershed.*

	3D subwatershed surface area	*mean valley bottom width*	*median bedrock depth*	*mean stream slope*	*most downstream stream temperature site*		
					elevation	*mean*	*7-d max*
site	(km^2)	(m)	(m)	(°)	(m)	(°C)	(°C)
Hughes River	42.2	73.7	1.52	22.7	307	18.7	21.2
Meadow Run	15.0	55.3	1.93	14.2	450	18.4	20.4
Jeremys Run	37.5	51.8	1.94	16.3	286	19.6	23.6
Hazel River	22.5	48.3	1.98	13.0	328	18.5	21.7
Paine Run	21.7	51.6	2.24	15.6	426	18.8	20.9
Whiteoak Cyn.	22.4	45.0	2.38	17.2	348	18.7	21.2
Piney River	20.6	48.6	2.54	14.9	371	17.9	20.6
Staunton River	18.0	45.6	3.43	20.7	309	17.4	19.9

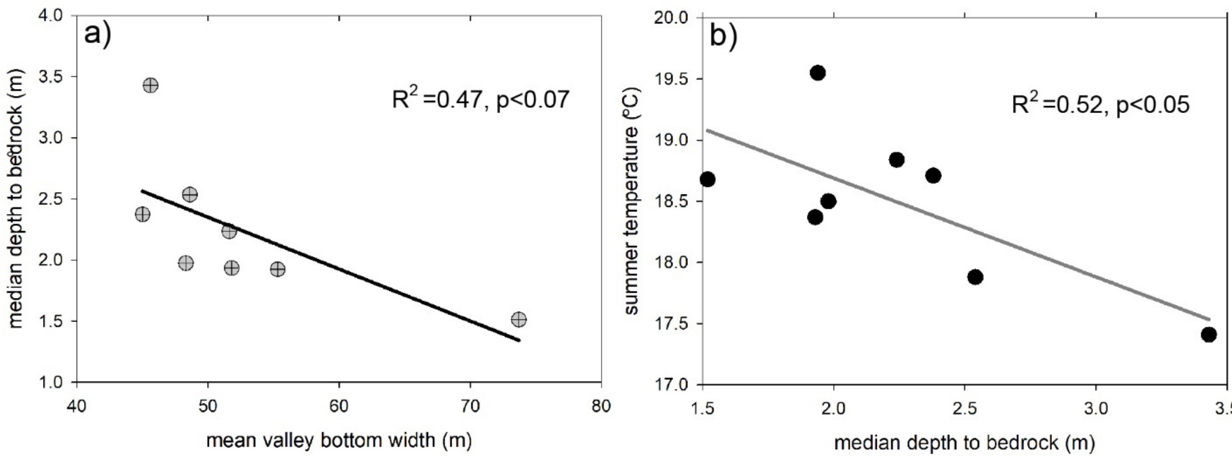

Figure 5. Median study stream corridor bedrock depth showed a negative relation to valley bottom width (panel a), and mean summer stream temperature at the lower study stream boundaries was negatively related to median bedrock depth (panel b).

4.2 Spatial Dewatering Patterns and Climate Data

Cumulative monthly precipitation during baseflow summer (July-September) was higher than normal in 2016 and near average or lower than average (period of record 1942-2020), depending on the month, in 2019 (Figure A2). Mean monthly air temperatures were higher than average for both study years during baseflow summer reflecting the long-term trend of increasing air temperatures in the park (Luray weather station GHCND:USC00445096). Patches of stream dewatering were observed along five of the eight study subwatersheds between 19-27 July, 2016, when over 98 km of total stream length were mapped (Figure 6). However, for Meadow Run, Hazel River, and Hughes River stream dewatering only occurred near the upper stream origination point. In contrast, Paine Run and Jeremys Run had several discrete dewatering sections further from their origination points (examples shown in Figure 3d, Figure A3). During the drier period 17-19 September 2019, no dewatering was found along lower Staunton River, though Piney River had seven discrete dry patches where none were mapped in 2016, and similar patterns were observed for those two streams in 2021 (Figure 7). Paine Run had 29 points of dewatering in 2019, distributed mainly along the central and upper sections of the stream corridor, and showed extensive dewatering in 2021 (Figures 6, 7, 8). The two Paine locations that were dry in 2016 were also dry in 2019 and 2021.

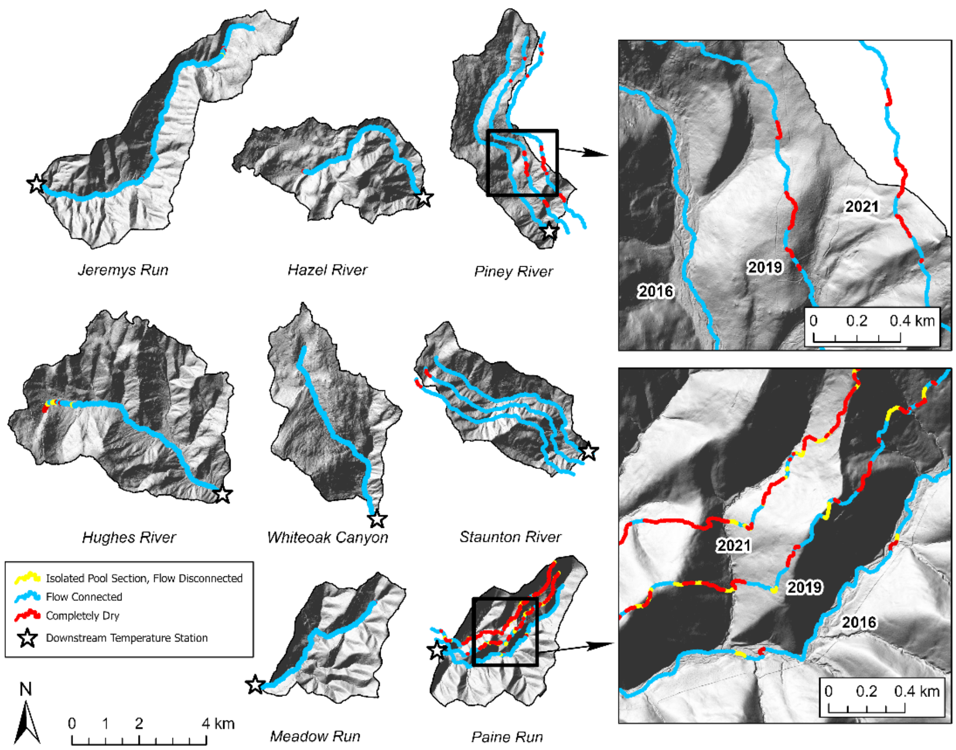

Figure 6. Results from 2016, 2019, and 2021 longitudinal channel dewatering surveys conducted by physical observation, where the 2019 and 2021 data are shown offset laterally from the stream channel where those surveys occurred.

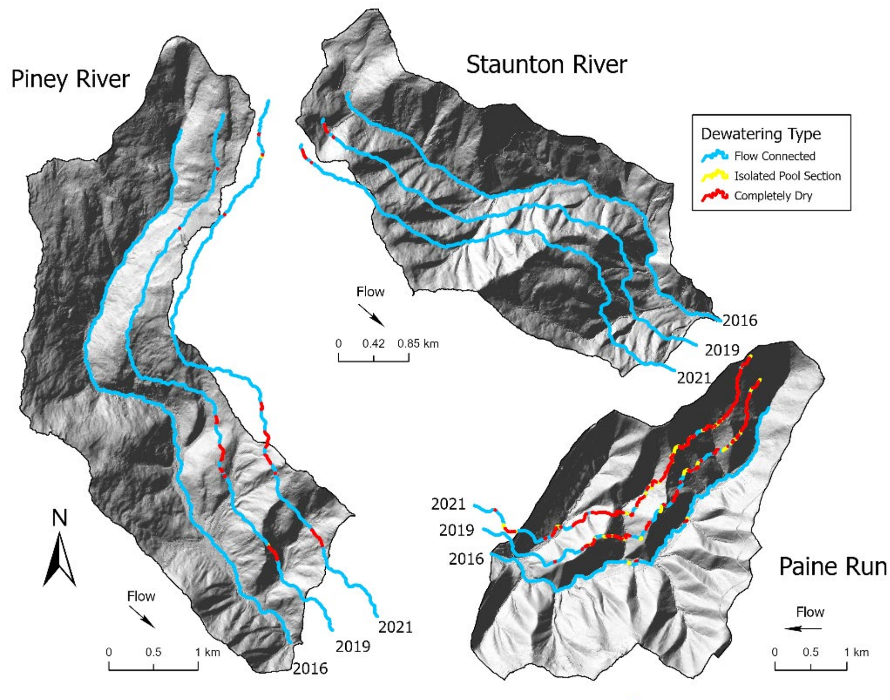

Figure 7. Zoom views for the three study subwatersheds where stream dewatering observations were also collected over three summer seasons (2016 ,2019, 2021).

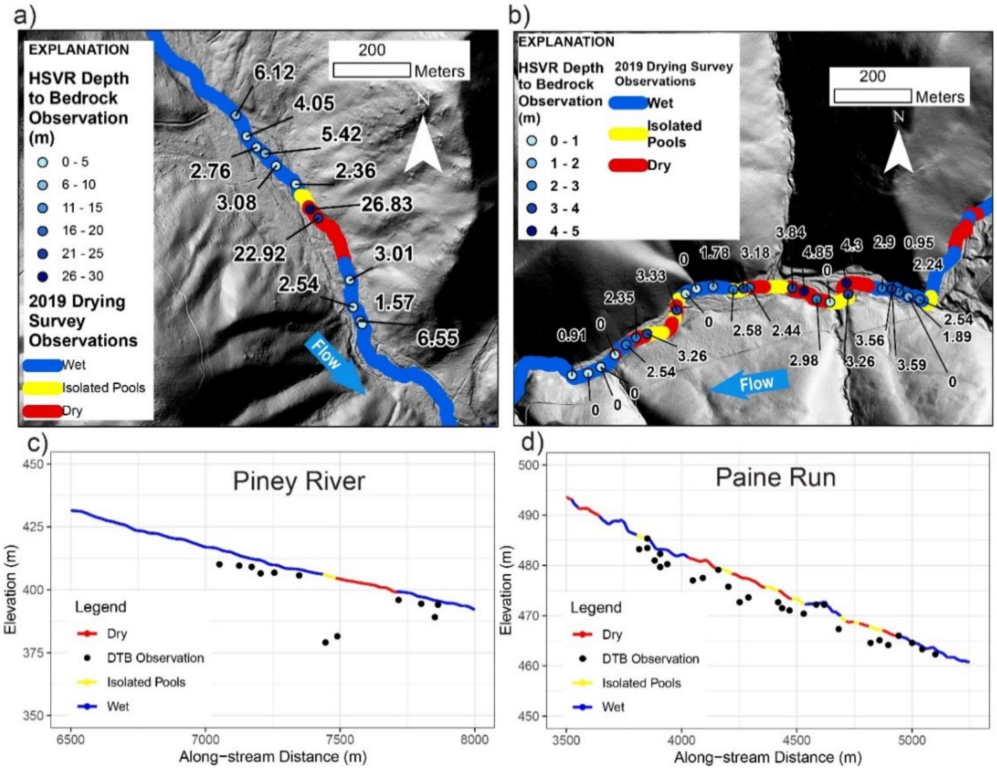

Figure 8. The results of the 2019 stream drying survey and 2020 high spatial resolution HVSR measurements are shown over the LiDAR hillshade in plan view (panels a, b) and along a LiDAR-derived stream elevation profile cross-section view (panels c, d) for Piney River (panels a, c) and Paine Run (panels b, d).

4.3 Stream Temperature Patterns

Paired air and water annual temperature signals exhibited a spectrum of shallow groundwater influences as indicated by extracting fundamental sinusoids from each multi-year temperature dataset per methods described by Briggs et al. (2018). Observed phase shifts between stream and local air temperature signals ranged from approximately 5 to 30 d with a mean of 11 d. Reduced annual temperature signal amplitude ratio generally corresponded with increased phase shift when all SNP stream monitoring sites are plotted in aggregate (Figure 9a). Staunton River stream sites cluster together and show less signal phase shift (mean of 10 d) for similarly low amplitude ratio values (mean of 0.6) observed in other subwatersheds.

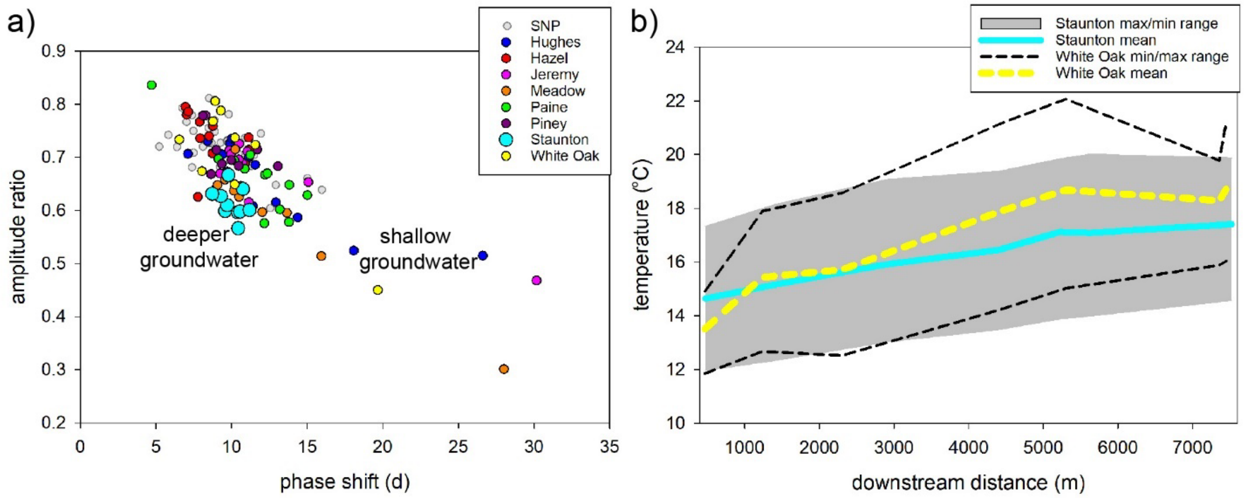

Figure 9. Panel a) shows the annual temperature signal metrics for the study subwatersheds highlighted within the larger SNP dataset with conceptual groundwater end member signature trajectories. Panel b) displays the downstream mean summer temperature profiles and 7-d maximum and minimum temperature ranges for Staunton River and Whiteoak Canyon.

Although originating in a similar place (Table 1), the downstream mean, 7-d maximum, and 7-d minimum stream temperature profiles differed between Staunton River and Whiteoak Canyon, where the latter had greater temperature variation and warming with downstream distance (Figure 9b). The mean summer stream temperature had an approximate 2 °C total range over the period of record. The warmest average (19.6 °C) and 7-d maximum (23.6 °C) was observed for the lower Jeremys Run site, which was also at the lowest elevation. However, only 23 m higher in elevation, the downstream Staunton River site had the coldest average (17.4 °C) and 7-d maximum (19.9 °C) summer temperature. Piney River, which has the second largest median bedrock depth (2.54 m), had the second lowest average temperature (17.4 °C) at the lower site. No significant relation was observed between elevation and mean summer temperature at the lower stream monitoring site, but a significant negative linear relation (R^2=0.52; p<0.05) was determined between median stream corridor bedrock depth and mean summer stream temperature (Figure 5b), with strong leverage on the linear fit imparted by the Staunton River datapoint.

4.4 Baseflow Separation (Index)

The summer season BFI determined for Paine Run, Piney River, and Staunton River over the period of flow record show substantial variability, but the median summer BFI for Staunton River (0.62) is approximately 50% greater than Paine Run and Piney River (0.46 and 0.41, respectively, Table 2). For the primary study years of 2016-2019, Staunton River BFI is always largest, and all sites are above their respective interquartile range in 2017 but below their interquartile range in 2018 (Figure 10). The anomalously low 2018 BFI values can be explained by extremely high summer precipitation that year (Figure S2), resulting in total streamflow being dominated by runoff and quickflow as determined by with baseflow separation. Mean summer streamflow over the period of record was highest for Piney River and lowest for Pain Run, and overall summer streamflow was most stable for Staunton River (lowest coefficient of variation).

Table 2. The median summer Baseflow Index (BFI), mean summer streamflow, and mean summer standard deviation (SD) streamflow for three gaged streams from 1993-2020.

site	*median BFI*	*mean streamflow* (L/s)	*mean coefficient of streamflow variation*
Paine Run	0.46	93.0	1.6
Piney River	0.41	164.4	1.7
Staunton River	0.62	157.3	0.7

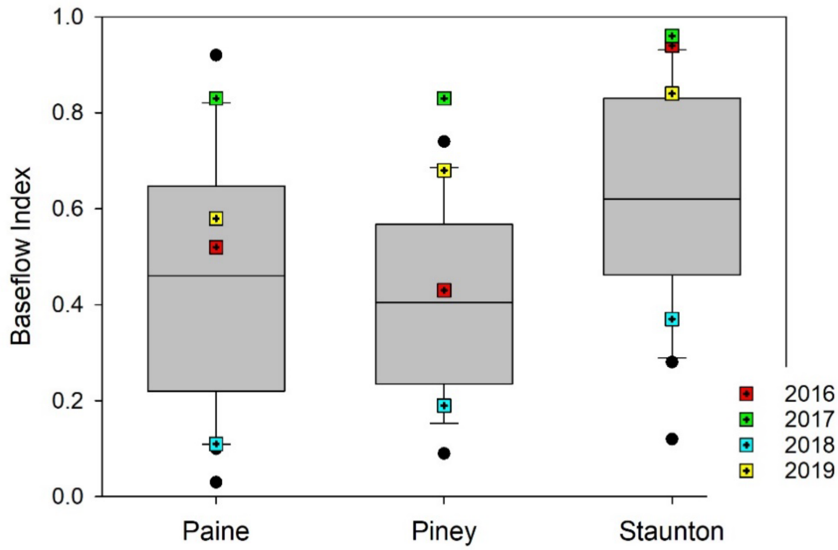

Figure 10. Summer Baseflow Index metrics summarized from 1993-2020 for three streams, with specific values from the primary study years identified.

5.0 Discussion

5.1 Longitudinal Spatial Structure in Observed Bedrock Depth

Seminal groundwater/surface water exchange research has indicated that bedrock topography along headwater streams may be a first-order control on the arrangement of nested gaining and losing flowpaths (e.g. Tonina & Buffington, 2009), and increased depth to low permeability bedrock contacts is recognized as a primary driver of stream disconnection during dry periods that could be exacerbated by climate change (Ward et al 2020). However, despite the apparent importance to a range of headwater stream physical processes and cold-water habitat, local bedrock depth data are almost universally lacking, even in heavily studied experimental watersheds. Our study provides new inferences regarding the effects of bedrock depth on groundwater exchange and consequent effects on stream dewatering and temperature patterns at ecologically relevant spatial scales in mountain streams. The combined datasets indicate stream channel bedrock depth assessments may be necessary to support stream habitat assessments and predictions of stream connectivity under drought and climate change when existing large-scale geologic datasets are not of sufficient spatial resolution to support natural resource management applications.

Bedrock depth varied substantially within and among several of the eight study SNP subwatersheds but was predominantly shallow. For half of the subwatersheds (Hughes River, Meadow Run, Jeremys Run, and Hazel River), median bedrock depth along the stream channel and lateral riparian zone was less than 2 m and did not show notable variability with distance, outside of one 12.8 m depth to rock location at upper Hazel River (Figure 4). This anomalous measurement at Hazel was collected lateral to the stream on a valley terrace of colluvium, in the vicinity of the only cold (approximately 10 °C at land surface) riparian spring that was observed during all HVSR surveys. Bedrock depths of greater than 8 m were found along the upper Whiteoak Canyon riparian zone as well (Briggs et al 2018a), also associated with surficial seepage. Two anomalous bedrock depth measurements of 22.9 and 26.8 m were collected along the Piney River channel, but instead of being associated with groundwater springs, they coincided with a discrete sections of channel dewatering at baseflow during 2019 and 2021. Therefore, it appears that discrete zones of thick surficial material are the exception along SNP streams, though they can be important to localized processes such as focused riparian discharge and streamflow disconnection (latter discussed in Section 5.2).

There are several existing sources of bedrock depth data that could potentially be used to inform headwater stream modeling and habitat assessment, but the accuracy of such datasets along headwater streams (typically away from existing boreholes) has generally not been evaluated. We conducted a point-scale comparison of our relatively high-resolution bedrock depth measurements to the global bedrock depth map of Shangguan et al., (2017) and found that bedrock depths were almost universally overpredicted at the SNP by large margins (Figure A4). Specifically, predictions from the global-scale dataset exceeded HVSR measured depths by +12.2 m (mean), or approximately four times the average bedrock depth (2.9 m). This result may not be surprising, as Shangguan et al., (2017) recognizes that large scale bedrock depth interpolations are likely to overpredict shallow bedrock contacts, especially in mountainous terrain with minimal available borehole data constraints. However, given that baseflow generation is expected to be dominated by shallow groundwater sourced from unconsolidated sediment in headwater systems with low permeability bedrock, our study highlights that use of large-scale bedrock depth layers may propagate substantial uncertainty into process-based groundwater flow model predictions when used to inform model structure in the absence of local measurements.

Publicly available maps of surficial geologic materials are another potential source of bedrock depth information. High-resolution digital soils maps are now widely available, including for the catchments of SNP, and these maps do capture some of the general depth to rock transitions between subwatersheds observed in this study. For example, NRCS (2020) (https://websoilsurvey.sc.egov.usda.gov/App/WebSoilSurvey.aspx, accessed 12/10/2020) indicate that the Whiteoak Canyon stream corridor is comprised of silts, loams, and stony soils with a general bedrock depth of approximately 1.2 m., which is in a similar range as most HVSR measurements made along the upper stream section (Figure 4). However, the generalized soil units may not offer needed detail regarding site-specific valley sediment thickness for hydrogeological and ecological studies where information regarding within-watershed variation is critical. Along lower Piney River, where HVSR data had depths to rock ranging 1.4 to 3.6 m, the NRCS soils map universally indicates silt and stony material > 2 m. Along Paine Run, where the stream is often scoured to bedrock, the soils map shows consistent highly permeable sandy material with > 2 m thickness. This discrepancy is understandable given most of the test pits were likely substantially further downstream in better terrain for agriculture. In conclusion, analysis of large-scale patterns from existing soils maps and interpolated/predicted bedrock depth layers indicates that more precise geophysical mapping of bedrock depth may be needed to inform stream research and management, particularly in shallow, low-permeability bedrock terrain.

5.2 Summer Stream Dewatering Related to Bedrock depth

Aligned with the conceptual model of Ward et al., (2018), our central hypothesis was bedrock depth along the stream corridor acts as a primary control on longitudinal stream dewatering and flow disconnection during summer low flows (visual example shown in Figure A3). We postulated that permeable streambed thickness may undulate along mountain stream channels, and relatively thick sub-stream sediment zones could accommodate the entirety of low streamflow volumes, locally disconnecting channels during seasonal flow recession. We found mixed support for this simple hypothesis. Hazel River and Hughes River were two of the three subwatersheds that had dry channel zones just downstream of their respective stream origination points in 2016, and these two riparian corridors also had their deepest riparian bedrock depths in those high-elevation areas. However, as discussed above, Whiteoak Canyon had relatively thick, porous sediment zone near the subwatershed outlet but did not show any zones of dewatering, nor did lower Staunton River in 2016, 2019, or 2021, despite having the deepest median bedrock contact. Jeremys Run had three mapped dry zones in 2016 (not surveyed in 2019), yet depth to rock in those areas was only approximately 2 m, though the HVSR data collection points were not perfectly aligned with the dry patches. To address this spatial mismatch in stream dewatering and HVSR data, we used the stream dewatering maps to guide two new high-resolution HVSR surveys in March 2020 along sections of Paine Run and Piney River with dynamic patterns of channel drying, as described below.

When bedrock depth data were collected at high-resolution, even more variability in bedrock topography/sediment thickness was revealed than in the original larger-scale surveys, and that finer scale of information was relevant to understanding stream dewatering patterns. For example, during summer 2019, a 291 m length section of lower Piney River was observed to be dry, and immediately preceded by 62 m of isolated stream channel pools, and a nearly identical dewatering pattern was observed there in 2021 (Figures 7,8a,c). The upper portion of this major feature of stream disconnection corresponded directly with a transition in bedrock depth along the channel from approximately 3 m to adjacent measurements of 27 and 23 m. This 'trough' in the bedrock surface can likely act as a streamwater sink (shown conceptually in Figure 1b), routing surface water downward to the point of draining the channel locally in the summers of 2019 and 2021, but not in 2016 when precipitation (groundwater supply) was higher than normal. Further downstream, the bedrock depth returned to approximately 3 m near the furthest downstream measurement point, and flowing channel water was again noted during the drying surveys. Such a section of stream dewatering in the lower watershed would serve to impede fish passage along Piney River during the lowest flows, likely corresponding to times of maximum thermal stress when fish mobility is critical to seeking thermal refuge (Magoulick and Kobza, 2003).

Not all variability in bedrock depth below streams associated with stream drying was as dramatic as the Piney River example but can be important in disconnecting channel habitat in summer. Paine Run is a more strongly confined stream valley that had 29 discrete zones of stream channel dewatering during September of 2019 and extensive dewatering in 2021 (Figures 6,7,8b,d), when numerous dead brook trout were also noted. Paine also had the greatest total exposed bedrock out of any of the SNP subwatersheds in this study, indicating a highly constrained valley underflow reservoir. High resolution bedrock depth data was collected over a Paine Run subreach with seven discrete dry patches ranging from 17 m to 185 m in channel length, with many bordered by zones of isolated pools (Figure 8b). A comparison of these patterns with bedrock depth along the channel shows the flowing sections of stream were dominated by exposed bedrock surfaces or thin sediment. However, a notable exception is toward the upstream end of this focus reach, where depth to rock was consistently > 2 m over the run up to a large zone of disconnected channel with some isolated pools (Figure 8b,d). This result suggests the losses of stream water accumulated over this approximately 80 m channel distance. In the following downstream contiguous sections of dry channel and/or isolated pools, bedrock depth averaged a larger 3.3 m, indicating the entirety of streamflow was accommodated by the subsurface, congruent with our original hypothesis. However, knowledge of bedrock depth in isolation is clearly not sufficient to predict stream channel gaining, losing, and disconnection patterns as the stream with the largest average bedrock depth, lower Staunton River (median depth to rock 3.4 m, Figure 4), was not observed to dewater during any of the three physical surveys (Figures 6,7).

5.3 Summer Stream Temperature and Groundwater Exchange Dynamics

Although headwater stream heat budgets are complex, our data indicates groundwater connectivity plays an important role when stream temperatures are already close to aquatic species thermal tolerances. The apparent dominance of shallow (<3 m depth) groundwater discharge along Whiteoak Canyon contributed to the Briggs et al. (2018b) prediction that the lower reaches would not provide suitable brook trout habitat by the end of the century given anticipated atmospheric warming. Jeremys Run, a long (13.4 km) stream consistently underlain by a shallow bedrock contact (median depth < 2 m), already shows a 7-d maximum summer temperature that exceeds expected brook trout tolerances (i.e., >23.3 °C mean weekly average temperature, Wehrly et al., (2007)) along the lowest reach.

The underflow reservoir of headwater stream valleys integrates upgradient and lateral hillslope groundwater flowpaths, which accumulate with distance when bounded by low permeability bedrock. The two subwatersheds with largest median bedrock depth along their respective upstream corridors had the coldest mean summer temperatures, with Staunton River standing out as distinctly colder, and having the only 7-d max temperature below 20 °C (Table 1). There was a significant relation between median bedrock depth and mean summer stream temperature at the lower stream sites but not with elevation (Figure 5b), indicating exchange with groundwater had disrupted the expected elevation control on lower reach cold water habitat. Surficial hillslope contributing area is often assumed a primary control on potential groundwater discharge at the stream subreach scale. However, Staunton River also had the second smallest drainage surface area of all study subwatersheds, and it is often assumed that lateral groundwater inflow to headwater streams is related to presumed upslope contributing area. Further, Staunton River did not have an average valley bottom width that was greater than other streams that were observed to dewater. This apparent conundrum indicates the importance of bedrock depth (suprabedrock aquifer thickness) in facilitating spatially persistent baseflow generation during dry times, and we also found that the more narrow headwater stream valleys of this study tended to have deeper bedrock depth (Figure 5a).

Our research indicates that the vertical shallow aquifer dimension, as represented by bedrock depth, is likely an important control of groundwater storage and connectivity to the stream corridor. This conclusion is supported by the paired air/water annual temperature signal metrics, indicating Staunton River sites cluster toward stronger, deeper groundwater influence compared to most observations along the other SNP streams (Figure 9a). Therefore, it seems there are important tradeoffs between bedrock depth along the stream channel as a driver of stream dewatering and sediment thickness along the valley floor and hillslopes as a potential source of stream baseflow.

For a more in-depth analysis of the paired bedrock depth and groundwater inflow controls on headwater summer stream dynamics, Staunton River can be contrasted with Paine Run. The latter had a similar total drainage surface area to Staunton River with a >5 m (average) wider stream valley bottom, but a 1.2 m shallower bedrock depth on average. Paine Run had dozens of dewatered stream channel sections in 2019 and 2021, and had a downstream boundary summer stream temperature that was 1.4 °C warmer than Staunton River. In addition to a reduced average bedrock depth, Paine Run had numerous sections of exposed bedrock adjacent to localized pockets of stream channel alluvium and colluvium (Figure 4, 7), while extensive colluvial deposits along the Staunton River channel limited exposed bedrock to a few m-scale sections associated with pool steps (Figure 4). Lower Staunton experienced major debris flows in June, 1995 (Morgan and Wieczorek, 1996), events that likely created an enhanced local groundwater reservoir within coarse hillslope material compared to other SNP subwatersheds.

Based on the integrated datasets from these two SNP streams, we conclude that groundwater exchange is a critical factor determining whether headwater streams will warm and dewater in summer, which in turn is controlled in part by the thickness of supra-bedrock unconsolidated aquifer. As noted above, annual temperature metrics indicated a consistently deeper groundwater discharge influence along Staunton River, while Paine Run had annual signal metrics that mainly indicated reduced and/or more shallow groundwater influence (Figure 9a). Long-term streamflow and baseflow analysis from these streams showed Staunton River had higher, but more stable summer discharge (Table 1), and substantially higher median summer BFI (0.62 vs 0.46), indicating greater dominance of groundwater as a generator of streamflow compared to runoff and quickflow. Previous research in SNP used paired air/stream water temperature records, precipitation, and landscape characteristics to statistically model 'groundwater influence' by year on a scale of 0-1 at the 100-m scale along the streams of this study, where details are described by Johnson et al., (2017). Although this previous work only extended to 2015, that year had analogous BFI scores to 2019 for Staunton River (0.88 vs 0.84) and Paine Run (0.60 vs 0.58). Comparing the 2019 drying survey observations to the 2015 high spatial resolution modeling of groundwater influence we found that Paine Run was predicted to have groundwater influenced tributaries, but along the mainstem, where extensive dewatering was observed, there was substantially reduced modeled groundwater influence compared to the mainstem of Staunton River (Figure 11). Johnson et al., (2017) also found a negative relation between valley bottom width and their metrics of groundwater influence on SNP streams. In the context of our finding that bedrock depth is negatively related to valley bottom width, we find further support for the hypothesis that thicker headwater stream valley sediments are influential to baseflow generation in low permeability bedrock settings.

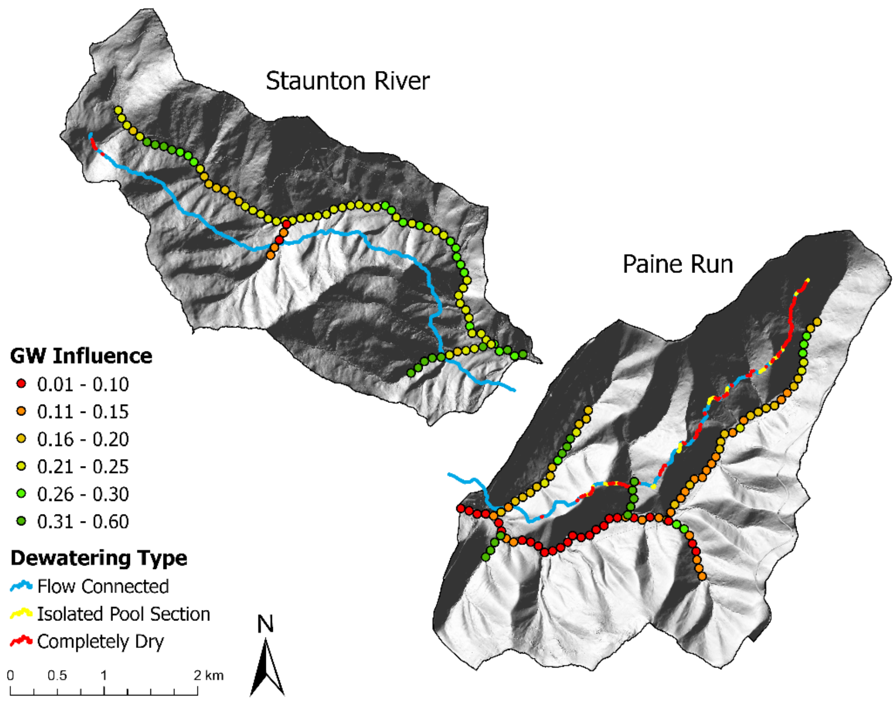

Figure 11. The 2019 stream dewatering survey data (lines; this study), plotted offset of the mainstem, and 100-m groundwater influence predictions (points from Johnson et al., 2017), plotted along the mainstem and tributaries, of Staunton River and Paine Run.

This observation and model comparison represents another line of evidence that groundwater connectivity at the sub-reach scale is key in determining whether local increases in depth to bedrock drive channel dewatering at low flow. The impact of reduced underflow groundwater supply on stream disconnection is likely exasperated by the extensive zones of exposed bedrock along Paine Run (Figure 4, 7d), which locally reduce groundwater mounding in stream valley sediments as shown conceptually in Figure 1b, such that abrupt increases in bedrock depth cause stream dewatering. Among the eight streams investigated here, Staunton River likely represents the most resilient summer cold water habitat, which could not be predicted using bedrock depth data alone but necessitated paired assessment of groundwater discharge dynamics.

6 Conclusions

In steep mountain valley stream systems underlain by low-permeability bedrock, the longitudinal underflow reservoir serves as a complex mechanism of streamflow generation, streamflow losses, and stream temperature control (Figure 1, Supplementary Figure S1). Our study utilized complimentary geophysical, temperature, and hydrologic data at the scale of eight subwatersheds to highlight apparent tradeoffs in bedrock depth, shallow groundwater supply, and the quality of cold-water habitat. Certain mountain stream corridor parameters may be reasonable to assume or infer from high-resolution topographic data, such as surficial sediment permeability (based on land surface roughness) and stream valley width, which are primary controls on whether underflow serves as a net source or sink of stream water (Flinchum et al., 2018; Ward et al., 2018). However, as shown here, advances in predicting hydrologic connectivity and thermal variation along mountain stream networks may also require local evaluation of bedrock depth and stream-groundwater exchange.

When local increases in bedrock depth are not balanced by groundwater inflow, streams may be expected to dewater and disconnect under low flow conditions, and streams with reduced deep groundwater influence or shallower-sourced groundwater show warmer summer temperatures. Contrary to what might be expected, we found that mean summer stream temperature was not significantly related to elevation at all lower study boundaries, but instead was (negatively) related to average stream bedrock depth. Staunton River had the coldest summer stream temperatures and most pronounced deeper groundwater signatures. However, that subwatershed was of relatively small total surface area and average valley bottom width. The defining physical feature of Staunton River was that it had the largest average bedrock depth of all the eight SNP study streams at 3.4 m, allowing greater overall storage of recharge and baseflow generation. The other two gaged streams had substantially reduced baseflow indices, indicating streamflow generation was dominated by runoff and quickflow.

Overall, SNP streams tended to have consistently shallow bedrock depth, though a subset were more variable or had spatial trends and discrete features. Observed channel dewatering patterns during late summer baseflow periods were related to local scale variation in bedrock depth, such as a discrete feature of greater than 20 m depth observed along Piney River that caused repeated streamflow disconnection. However, in other streams more subtle bedrock depth variation also caused channel dewatering, indicating the importance of local hydrogeological context in determining the importance of bedrock depth on streamflow connectivity. For example, patchy 2-4 m deposits of sediment adjacent to exposed bedrock along Paine Run caused extensive summer dewatering in 2019 and 2021, and during the latter survey many dead brook trout were noted in the disconnected sections. Paine and Piney also showed enhanced dewatering during the summers of 2019 and 2021 compared to the wetter 2016 summer, demonstrating the additional control of recent precipitation on stream disconnection in headwater systems that do not efficiently store water.

Lateral groundwater inflow through high permeability, unconsolidated sediments is a critical component of headwater stream baseflow (Tran et al., 2020). Shallow, low permeability bedrock can constrain lateral flowpaths and underflow to the near surface critical zone, where it is highly sensitive to enhanced evapotranspiration, temperature increase, and drought under climate change (Condon et al., 2020; Hare et al., 2021). As it becomes increasingly important to understand and predict the resilience of mountain cold-water stream habitat at a fine spatial grain, continued coupled advances in geophysical characterization, stream temperature monitoring, and groundwater exchange analysis are needed.

Data Availability

The data described in this manuscript are available at: doi.org/10.5066/F7B56H72, doi.org/10.5066/F7JW8C04, and doi.org/10.5066/P9IJMGIB

Author contribution

Conceptualization: M.A. Briggs, Z.C. Johnson, C.D. Snyder, N.P. Hitt; *Investigation*: M.A. Briggs, P. Goodling, Z.C. Johnson, C.D. Snyder, K.M. Rogers, N.P. Hitt; *Visualization*: M.A. Briggs, K.M. Rogers, P. Goodling, J.B. Fair, C.D. Snyder. All authors contributed to the formal analysis and varied stages of writing.

Competing interests

The authors declare that they have no conflict of interest.

Acknowledgments

The authors gratefully acknowledge support from Natural Resource Preservation Program and the U.S. Geological Survey (USGS) Chesapeake Bay Priority Ecosystems Science and Fisheries Program. We also thank the Shenandoah National Park Staff for site access and general support and field support from John Lane, David Nelms, Adam Haynes, Erin Snook, David Weller, Evan Rodway, Jacob Roach, Matt Marshall, Joe Dehnert, and Mary Mandt. Any use of trade, firm, or product names is for descriptive purposes only and does not imply endorsement by the U.S. Government.

References

Barlow, P.M., Cunningham, W.L., Zhai, T., Gray, M., 2014. U.S. Geological Survey Groundwater Toolbox, a graphical and mapping interface for analysis of hydrologic data (version 1.0): User guide for estimation of base flow, runoff, and groundwater recharge from streamflow data: U.S. Geological Survey Techniques a. B. 3 B10, 27. https://doi.org/http://dx.doi.org/10.3133/tm3B10

Briggs, M.A., Johnson, Z.C., Snyder, C.D., Hitt, N.P., Kurylyk, B.L., Lautz, L., Irvine, D.J., Hurley, S.T., Lane, J.W., 2018a. Inferring watershed hydraulics and cold-water habitat persistence using multi-year air and stream temperature signals. Sci. Total Environ. 636. https://doi.org/10.1016/j.scitotenv.2018.04.344

Briggs, M.A., Lane, J.W., Snyder, C.D., White, E.A., Johnson, Z.C., Nelms, D.L., Hitt, N.P., 2018b. Shallow bedrock limits groundwater seepage-based headwater climate refugia. Limnologica 68, 142–156. https://doi.org/10.1016/j.limno.2017.02.005

Briggs, M.A., Lane, J.W., Snyder, C.D., White, E.A., Johnson, Z.C., Nelms, D.L., Hitt, N.P., 2017. Seismic data for study of shallow mountain bedrock limits seepage-based headwater climate refugia, Shenandoah National Park, Virginia: U.S. Geological Survey data release. https://doi.org/10.5066/F7JW8C04

Bundschuh, J., 1993. Modeling annual variations of spring and groundwater temperatures associated with shallow aquifer systems Computer model. J. Hydraul. Eng. 142, 427–444.

Burns, D.A., Murdoch, P.S., Lawrence, G.B., Michel, R.L., 1998. Effect of groundwater springs on NO3/- concentrations during summer in Catskill Mountain streams. Water Resour. Res. 34, 1987–1996. https://doi.org/Cited By (since 1996) 98Export Date 4 April 2012

Condon, L.E., Atchley, A.L., Maxwell, R.M., 2020. Evapotranspiration depletes groundwater under warming over the contiguous United States. Nat. Commun. 11. https://doi.org/10.1038/s41467-020-14688-0

Costigan, K.H., Jaeger, K.L., Goss, C.W., Fritz, K.M., Goebel, P.C., 2016. Understanding controls on flow permanence in intermittent rivers to aid ecological research: integrating meteorology, geology and land cover. Ecohydrology 9, 1141–1153. https://doi.org/10.1002/eco.1712

Covino, T., 2017. Hydrologic connectivity as a framework for understanding biogeochemical flux through watersheds and along fluvial networks. Geomorphology 277, 133–144. https://doi.org/10.1016/j.geomorph.2016.09.030

DeKay, R.H., 1972. Development of ground-water supplies in Shenandoah National Park, Virginia. Virginia Div. Miner. Resour. Rep. 10, 158.

Edge, C.B., Fortin, M.J., Jackson, D.A., Lawrie, D., Stanfield, L., Shrestha, N., 2017. Habitat alteration and habitat fragmentation differentially affect beta diversity of stream fish communities. Landsc. Ecol. 32, 647–662. https://doi.org/10.1007/s10980-016-0472-9

Fausch, K.D., Torgersen, C.E., Baxter, C. V., Li, H.W., 2002. Landscapes to riverscapes: Bridging the gap between research and conservation of stream fishes. Bioscience 52, 483–498. https://doi.org/10.1641/0006-3568(2002)052[0483:LTRBTG]2.0.CO;2

Flinchum, B.A., Holbrook, W.S., Grana, D., Parsekian, A.D., Carr, B.J., Hayes, J.L., Jiao, J., 2018. Estimating the water holding capacity of the critical zone using near-surface geophysics. Hydrol. Process. 32, 3308–3326. https://doi.org/10.1002/hyp.13260

Furze, S., Sullivan, A.M.O., Allard, S., Pronk, T., Curry, R.A., 2021. A High-Resolution , Random Forest Approach to Mapping Depth-to-Bedrock across Shallow Overburden and Post-Glacial Terrain. Remote Sens. 13, 1–23. https://doi.org/10.3390/rs13214210

Goodling, P.J., Briggs, M.A., White, E.A., Johnson, Z.C., Haynes, A.B., Nelms, D.L., Lane, J.W., 2020. Passive seismic data collected along headwater stream corridors in Shenandoah National Park in 2016 - 2020: US Geol. Surv. Data Release. https://doi.org/doi.org/10.5066/P9IJMGIB

Hare, D.K., Helton, A.M., Johnson, Z.C., Lane, J.W., Briggs, M.A., 2021. Continental-scale analysis of shallow and deep groundwater contributions to streams. Nat. Commun. 1–10. https://doi.org/10.1038/s41467-021-21651-0

Herzog, S.P., Ward, A.S., Wondzell, S.M., 2019. Multiscale Feature-feature Interactions Control Patterns of Hyporheic Exchange in a Simulated Headwater Mountain Stream. Water Resour. Res. 55, 10976–10992. https://doi.org/10.1029/2019WR025763

Hopper, G.W., Gido, K.B., Pennock, C.A., Hedden, S.C., Frenette, B.D., Barts, N., Hedden, C.K., Bruckerhoff, L.A., 2020. Nowhere to swim: interspecific responses of prairie stream fishes in isolated pools during severe drought. Aquat. Sci. 82, 1–15. https://doi.org/10.1007/s00027-020-0716-2

Ilja Van Meerveld, H.J., Kirchner, J.W., Vis, M.J.P., Assendelft, R.S., Seibert, J., 2019. Expansion and contraction of the flowing stream network alter hillslope flowpath lengths and the shape of the travel time distribution. Hydrol. Earth Syst. Sci. 23, 4825–4834. https://doi.org/10.5194/hess-23-4825-2019

Jencso, K.G., McGlynn, B.L., Gooseff, M.N., Bencala, K.E., Wondzell, S.M., 2010. Hillslope hydrologic connectivity controls riparian groundwater turnover: Implications of catchment structure for riparian buffering and stream water sources. Water Resour. Res. 46, 1–18. https://doi.org/10.1029/2009WR008818

Johnson, Z.C., Johnson, B.G., Briggs, M.A., Devine, W.D., Snyder, C.D., Hitt, N.P., Hare, D.K., Minkova, T. V., 2020. Paired air-water annual temperature patterns reveal hydrogeological controls on stream thermal regimes at watershed to continental scales. J. Hydrol. 587, 124929. https://doi.org/10.1016/j.jhydrol.2020.124929

Johnson, Z.C., Snyder, C.D., Hitt, N.P., 2017. Landformfeatures and seasonal precipitation predict shallow groundwater influence on temperature in headwater streams. Water Resour. Res. 53, 5788–5812. https://doi.org/10.1002/2017WR020455

Kauffman, L.J., Yager, R.M., Reddy, J.E., 2018. Sediment and Aquifer Characteristics of Quaternary Sediments in the Glaciated Conterminous United States: U.S. Geol. Surv. data release. https://doi.org/10.5066/F7HH6J8X

Labbe, T.R., Fausch, K.D., 2000. Dynamics of intermittent stream habitat regulate persistence of a threatened fish at multiple scales. Ecol. Appl. 10, 1774–1791. https://doi.org/10.1890/1051-0761

Lapham, W.W., 1989. Use of temperature profiles beneath streams to determine rates of vertical ground-water flow and vertical hydraulic conductivity. US Geol. Surv. Water-Supply Pap. 2337.

Larkin, R.G., Sharp, J.M., 1992. On the relationship between river-basin geomorphology, aquifer hydraulics, and ground-water flow direction in alluvial aquifers. Geol. Soc. Am. Bull. 104, 1608–1620.

Litwin, D.G., Tucker, G.E., Barnhart, K.R., Harman, C.J., 2022. Groundwater Affects the Geomorphic and Hydrologic Properties of Coevolved Landscapes. J. Geophys. Res. Earth Surf. 127, 1–36. https://doi.org/10.1029/2021JF006239

Lynch, D.D., 1987. Hydrologic conditions and trends in Shenandoah National Park, Virginia, 1983–84. Water- Resour. Investig. Rep. 87–4131.

Magoulick, D.D., Kobza, R.M., 2003. The role of refugia for fishes during drought: A review and synthesis. Freshw. Biol. 48, 1186–1198. https://doi.org/10.1046/j.1365-2427.2003.01089.x

McLachlan, P.J., Chambers, J.E., Uhlemann, S.S., Binley, A., 2017. Geophysical characterisation of the groundwater–surface water interface. Adv. Water Resour. 109, 302–319. https://doi.org/10.1016/j.advwatres.2017.09.016

Meisner, J.D., Rosenfeld, J.S., Regier, H.A., 1988. The Role of Groundwater in the Impact of Climate Warming on Stream Salmonines. Fisheries 13, 2–8.

Nelms, D.L., Moberg, R.M., 2010. Preliminary Assessment of the Hydrogeology and Groundwater Availability in the Metamorphic and Siliciclastic Fractured-Rock Aquifer Systems of Warren County, Virginia. U.S. Geol. Surv. Investig. Rep. 2010–5190.

O'Sullivan, A.M., Devito, K.J., Ogilvie, J., Linnansaari, T., Pronk, T., Allard, S., Curry, R.A., 2020. Effects of Topographic Resolution and Geologic Setting on Spatial Statistical River Temperature Models. Water Resour. Res. 56, 1–23. https://doi.org/10.1029/2020WR028122

Odom, W.E., Doctor, D.H., Burke, C.E., Cox, C.L., 2021. Using high-resolution LiDAR and deep learning models to generate mimum thickness maps of surficial sediments, in: Geological Society of America Abstracts with Programs, v. 53. Portland, OR. https://doi.org/10.1130/abs/2021AM-367681

Payn, R.A., Gooseff, M.N., McGlynn, B.L., Bencala, K.E., Wondzell, S.M., 2009. Channel water balance and exchange with subsurface flow along a mountain headwater stream in Montana, United States. Water Resour. Res. 45. https://doi.org/Artn W11427Doi 10.1029/2008wr007644

Pelletier, J.D., Broxton, P.D., Hazenberg, P., Zeng, X., Troch, P.A., Niu, G.-Y., Williams, Z., Brunke, M.A., Gochis, D., 2016. A gridded global data set of soil, intact regolith, and sedimentary deposit thicknesses for regional and global land surface modeling. J. Adv. Model. Earth Syst. 8. https://doi.org/10.1002/2015MS000526

Plummer, L.N., Busenberg, E., Bohlke, J.K., Nelms, D.L., Michel, R.L., Schlosser, P., 2001. Groundwater residence times in Shenandoah National Park, Blue Ridge Mountains, Virginia, USA: a multi-tracer approach. Chem. Geol. 179, 93–111.

Rolls, R.J., Leigh, C., Sheldon, F., 2012. Mechanistic effects of low-flow hydrology on riverine ecosystems: Ecological principles and consequences of alteration. Freshw. Sci. 31, 1163–1186. https://doi.org/10.1899/12-002.1

Shangguan, W., Hengl, T., Mendes de Jesus, J., Yuan, H., Dai, Y., 2017. Mapping the global depth to bedrock for land surface modeling. J. Adv. Model. Earth Syst. 9, 65–88. https://doi.org/10.1002/2016MS000686

Sidle, R.C., Tsuboyama, Y., Noguchi, S., Hosoda, I., Fujieda, M., Shimizu, T., 2000. Stormflow generation in steep forested headwaters: A linked hydrogeomorphic paradigm. Hydrol. Process. 14, 369–385. https://doi.org/10.1002/(SICI)1099-1085(20000228)14:3<369::AID-HYP943>3.0.CO;2-P

Singha, K., Navarre-Sitchler, A., 2021. The importance of groundwater in critical zone science. Groundwater 1–8. https://doi.org/10.1111/gwat.13143

Snyder, C.D., Hitt, N.P., Johnson, Z.C., 2017. Air-water temperature data for the study of groundwater influence on stream thermal regimes in Shenandoah National Park, Virginia: U.S. Geological Survey data release. https://doi.org/https://doi.org/10.5066/F7B56H72

Snyder, C.D., Hitt, N.P., Young, J.A., 2015. Accounting for groundwater in stream fish thermal habitat responses to climate change. Ecol. Appl. 00, 281–304.

Snyder, C.D., Webb, J.R., Young, J.A., Johnson, Z.B., Jewell, S., Survey, U.S.G., 2013. Significance of Headwater Streams and Perennial Springs in Ecological Monitoring in Shenandoah National Park. Open-File Rep. 2013–1178 46.

Southworth, S., Aleinikoff, J.N., Bailey, C.M., Burton, W.C., Crider, E.A., Hackley, P.C., Smoot, J.P., Tollo, R.P., 2009. Geologic Map of the Shenandoah National Park Region, Virginia. US Geol. Surv. Open-File Rep. 2009–1153 1.

Stonestrom, D.A., Constantz, J., 2003. Heat as a Tool for Studying the Movement of Ground Water Near Streams. U.S. Geol. Surv. Circ., 1260, 1–6. 96.

Sullivan, C., Vokoun, J., Helton, A., Briggs, M.A., Kurylyk, B., 2021. An ecohydrological typology for thermal refuges in streams and rivers. Ecohydrology. https://doi.org/10.1002/eco.2295

Tiwari, T., Buffam, I., Sponseller, R.A., Laudon, H., 2017. Inferring scale-dependent processes influencing stream water biogeochemistry from headwater to sea. Limnol. Oceanogr. 62, S58–S70. https://doi.org/10.1002/lno.10738

Tonina, D., Buffington, J.M., 2009. Hyporheic Exchange in Mountain Rivers I: Mechanics and Environmental Effects. Geogr. Compass 3, 1063–1086. https://doi.org/10.1111/j.1749-8198.2009.00226.x

Tran, H., Zhang, J., Cohard, J.M., Condon, L.E., Maxwell, R.M., 2020. Simulating Groundwater-Streamflow Connections in the Upper Colorado River Basin. Groundwater 58, 392–405. https://doi.org/10.1111/gwat.13000

Ward, A.S., Schmadel, N.M., Wondzell, S.M., 2018. Simulation of dynamic expansion, contraction, and connectivity in a mountain stream network. Adv. Water Resour. 114, 64–82. https://doi.org/10.1016/j.advwatres.2018.01.018

Ward, A.S., Wondzell, S.M., Schmadel, N.M., Herzog, S.P., 2020. Climate Change Causes River Network Contraction and Disconnection in the H.J. Andrews Experimental Forest, Oregon, USA. Front. Water 2, 1–10. https://doi.org/10.3389/frwa.2020.00007

Warix, S.R., Godsey, S.E., Lohse, K.A., Hale, R.L., 2021. Influence of groundwater and topography on stream drying in semi-arid headwater streams. Hydrol. Process. 35, 1–18. https://doi.org/10.1002/hyp.14185

Weekes, A.A., Torgersen, C.E., Montgomery, D.R., Woodward, A., Bolton, S.M., 2015. Hydrologic response to valley-scale structure in alpine headwaters. Hydrol. Process. 29, 356–372. https://doi.org/10.1002/hyp.10141

Wehrly, K., Wang, L., Mitro, M., 2007. Field-based estimates of thermal tolerance limits for trout: incorporating exposure time and temperature fluctuation. Trans. Am. Fish. Soc. 136, 365–374.

Winter, T.C., Harvey, J.W., Franke, O.L., Alley, W.M., 1998. Ground water and surface water: a single resource. U. S. Geol. Surv. Circ. 1139 79.

Wohl, E., 2017. Connectivity in rivers. Prog. Phys. Geogr. 41, 345–362. https://doi.org/10.1177/0309133317714972

Wu, L., Gomez-Velez, J.D., Krause, S., Singh, T., Wörman, A., Lewandowski, J., 2020. Impact of Flow Alteration and Temperature Variability on Hyporheic Exchange. Water Resour. Res. 56. https://doi.org/10.1029/2019WR026225

Yanamaka, H., Takemura, M., Ishida, H., Niwa, M., 1994. Characteristics of long-period microtremors and their applicability in exploration of deep sedimentary layers. Bull. Seism. Soc. Am. 84, 1831–1841.

Zimmer, M.A., McGlynn, B.L., 2017. Bidirectional stream–groundwater flow in response to ephemeral and intermittent streamflow and groundwater seasonality. Hydrol. Process. 31, 3871–3880. https://doi.org/10.1002/hyp.11301

Appendix A

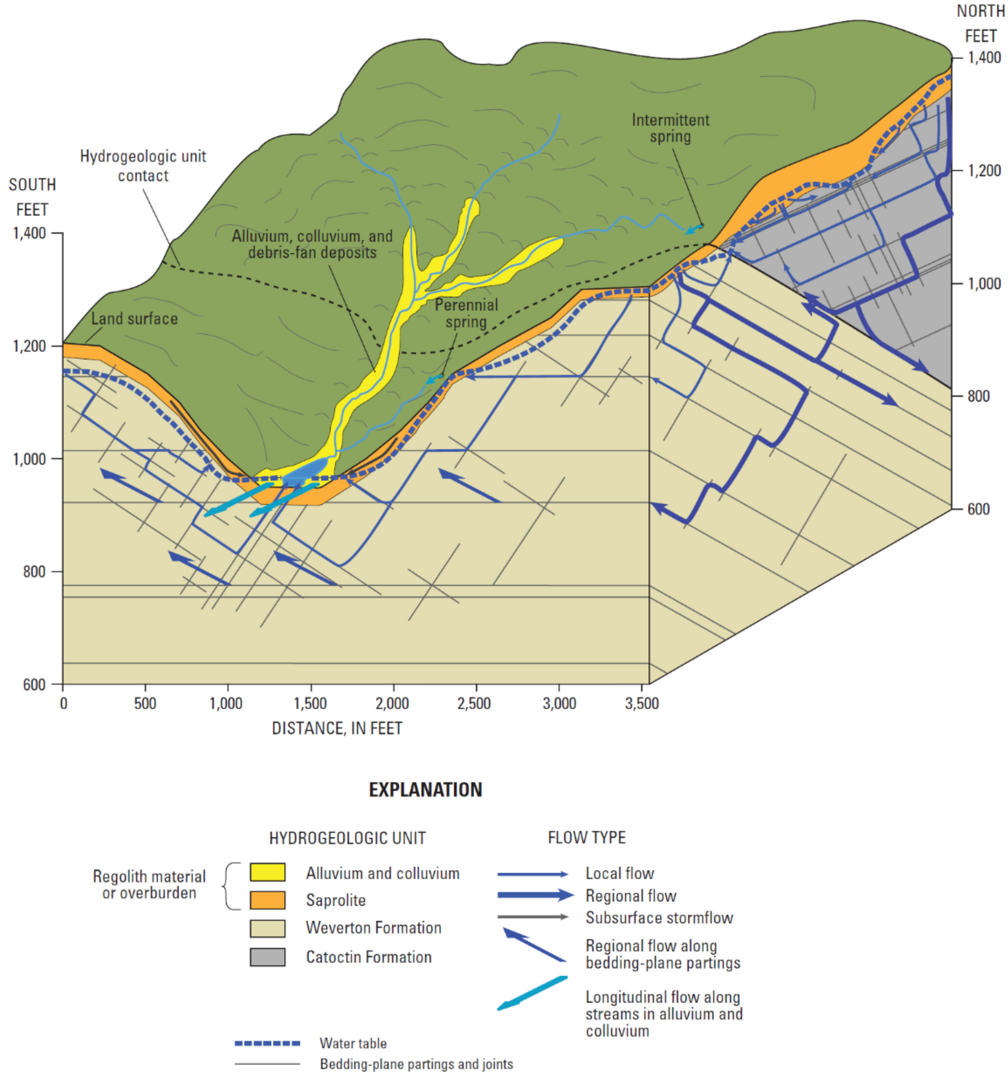

Figure A1. The headwater streams of Shenandoah National Park, Virginia, USA are expected to flow over coarse alluvium and colluvium and have connectivity to shallow hillslope groundwater and underflow, but reduced connectivity to deeper bedrock groundwater (Modified Figure 26 in (Nelms and Moberg, 2010) *U.S. Geol. Surv. Investigations Rep.* 2010–5190.

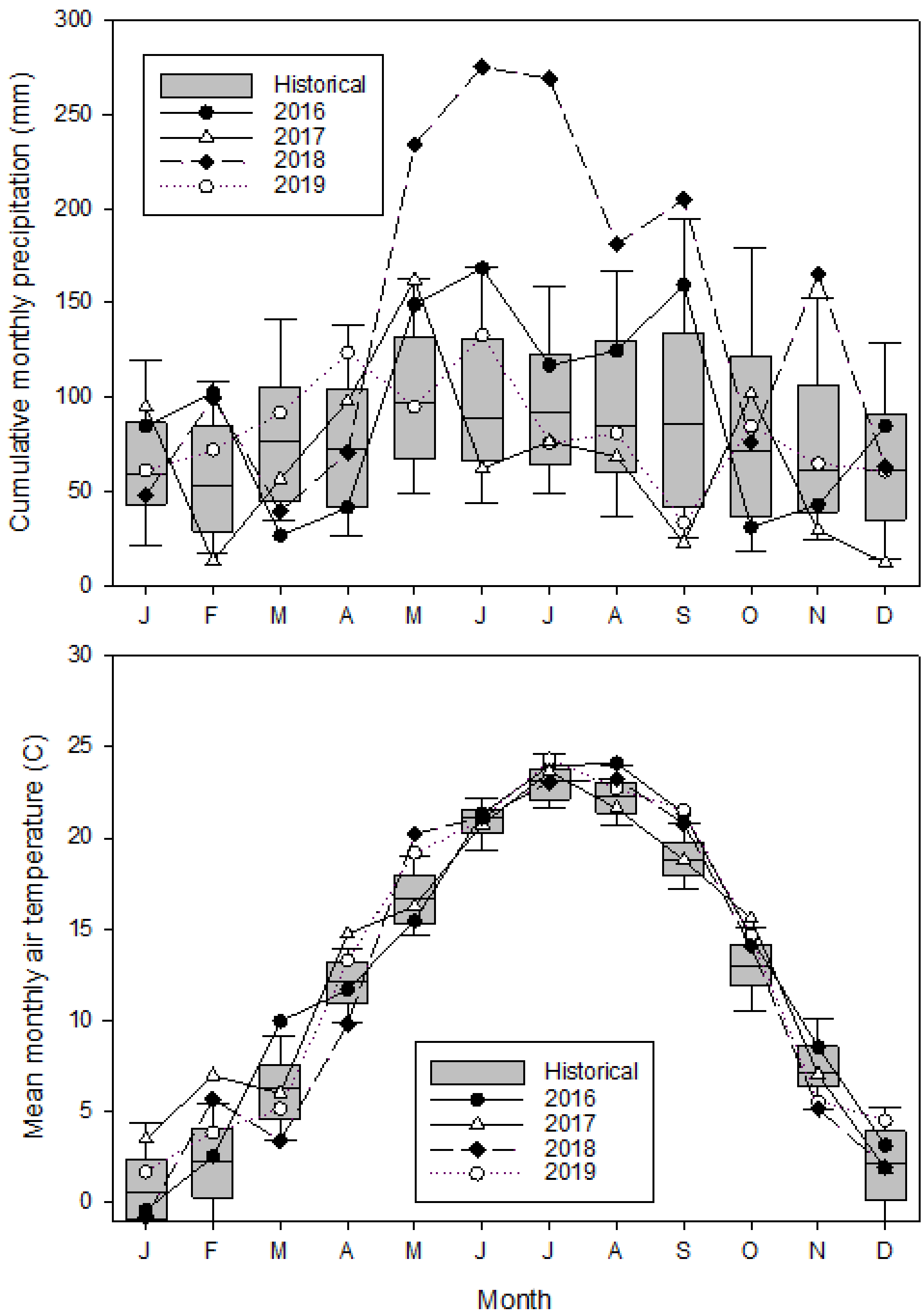

Figure A2. Monthly precipitation and air temperature data derived from the Luray weather station (GHCND:USC00445096) located within Shenandoah National Park. Box plots show the distribution of values for the period of record (1942-2020) with the limits of the box containing 50% of the values, whiskers containing 90% of the values, and solid line in boxes depicting the median value. The lines represent values for the four primary study years.

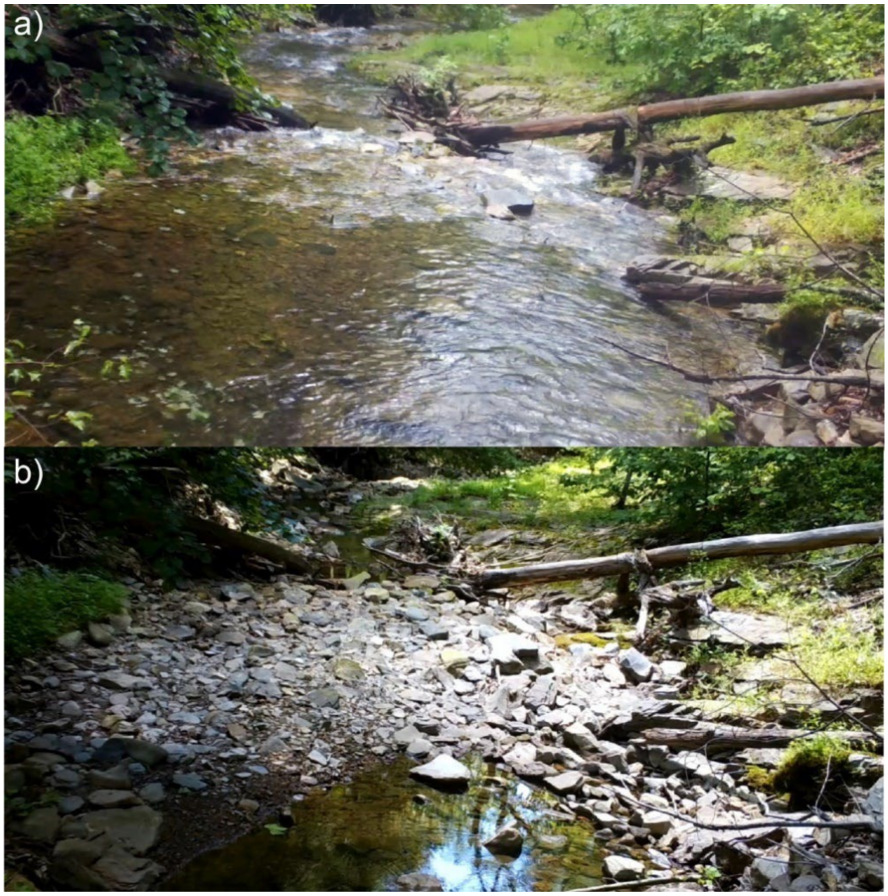

Figure A3. Images from the same vantage point along Paine Run during a) high and b) low flow times, the latter showing channel dewatering associated with a deposit of coarse alluvium across the channel.

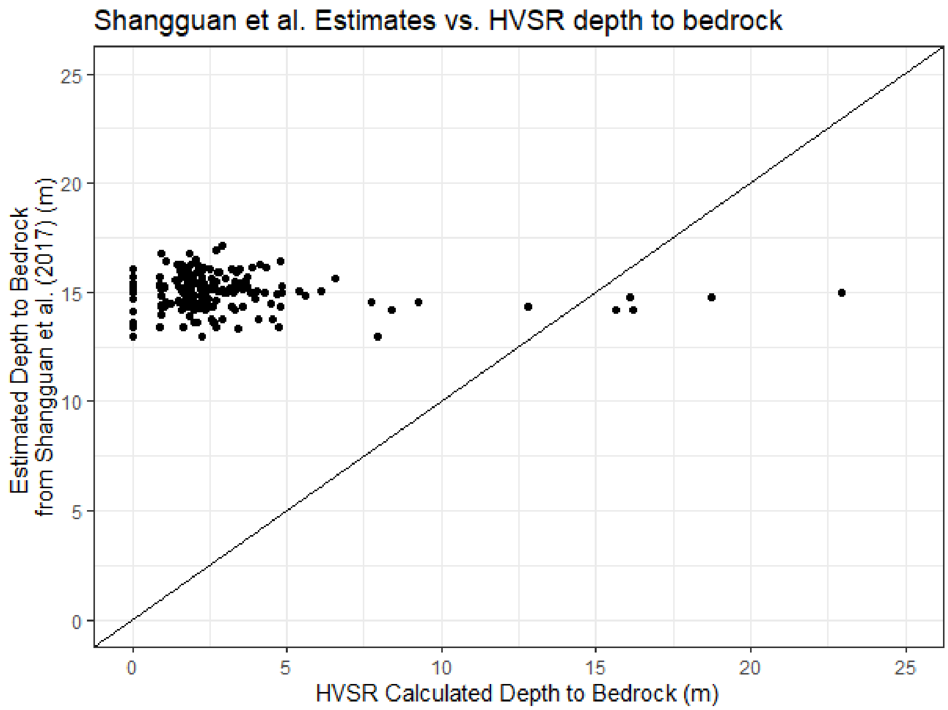

Figure A4: Comparison between bedrock depth modeled for the globe by Shangguan et al., (2017) at a 250m resolution and the HVSR-calculated depths to bedrock in this study.

Appendix B

Table B1. Summer stream temperature metrics for each study subwatershed determined from the data set of Snyder et al. (2017), doi.org/10.5066/F7B56H72.

Subwatershed	SiteID	Easting	Northing	Downstream Distance (m)	summer mean (°C)	7-d min (°C)	7-d max (°C)	Stdev (°C)
Hughes	HUR1MP	730038	4276000	242.50	13.43	11.50	16.07	0.98
Hughes	HUR3LCP	731058	4275970	1634.44	15.73	13.23	18.21	1.24
Hughes	HUR5LCP	732278	4275850	3308.93	16.21	13.48	18.62	1.24
Hughes	HUR6MP	733348	4275060	5163.46	16.39	13.86	17.95	1.13
Hughes	HUR12MP	733698	4274880	5620.73	16.79	14.09	18.34	1.24
Hughes	HUR8LCP	733988	4274619	6219.50	18.80	15.19	21.49	1.57
Hughes	HUR9LCP	733968	4274529	6284.35	17.59	14.49	20.09	1.34
Hughes	HUR10MP	734928	4273520	8187.04	18.05	15.01	20.05	1.40
Hughes	HUR13MP	735258	4273330	8667.16	18.68	15.15	21.18	1.62
Hazel	HZR1MP	735158	4278560	707.45	16.80	13.26	19.75	1.46
Hazel	HZR3LCP	735498	4278760	1190.18	16.74	13.08	19.41	1.50
Hazel	HZR11MP	736378	4279640	2951.89	18.16	15.34	20.32	1.52

Hazel	HZR5MP	736638	4279790	3331.66	17.59	13.59	20.62	1.67
Hazel	HZR6MP	737498	4279059	5095.01	18.16	14.03	21.40	1.74
Hazel	HZR7MP	738048	4277990	6820.13	18.48	14.50	21.77	1.72
Hazel	HZR9MP	738368	4277620	7478.33	18.50	14.74	21.72	1.63
Jeremys	JR1MP	734618	4293430	102.97	15.48	12.42	18.74	1.41
Jeremys	JR2MP	733908	4293130	1268.08	16.49	13.38	19.42	1.38
Jeremys	JR4MP	732498	4292250	3699.53	16.84	14.23	18.22	1.11
Jeremys	JR5MP	731778	4290670	5961.22	17.54	14.15	20.24	1.43
Jeremys	JR13MP	731498	4289490	7506.87	18.16	14.57	21.28	1.67
Jeremys	JR7MP	730068	4288080	10327.83	18.76	16.79	21.07	1.10
Jeremys	JR9LCP	729888	4288080	10539.49	17.78	15.33	20.01	1.04
Jeremys	JR12MP	728758	4288080	12030.09	18.61	14.46	22.08	1.73
Jeremys	JR10MP	727758	4288440	13376.47	19.55	14.93	23.55	1.98
Meadow	MR0MP	695318	4228150	0.00	14.16	12.01	15.57	1.07
Meadow	MR1MP	695038	4227980	217.46	16.82	13.82	18.39	1.28
Meadow	MR2MP	694678	4227520	979.43	17.11	13.71	18.78	1.48
Meadow	MR9MP	693488	4227270	2757.87	18.10	15.34	19.71	1.31
Meadow	MR4LCP	693428	4227240	2854.69	17.01	13.92	19.02	1.44
Meadow	MR8MP	693078	4226450	4036.50	17.53	14.32	19.48	1.35
Meadow	MR6LCP	692918	4226170	4446.20	17.08	14.34	19.32	1.29
Meadow	MR7MP	691738	4225700	6209.68	18.37	15.33	20.44	1.44
Paine	PAR1MP	696938	4232031	249.71	16.86	13.96	18.72	1.36
Paine	PARB1	696718	4231390	1115.08	17.20	14.81	18.70	1.15
Paine	PAR2MP	696468	4231210	1542.16	17.15	15.22	18.61	1.03
Paine	PAR3MP	695685	4230400	3169.18	17.48	14.93	19.28	1.15
Paine	PAR5LCP	695369	4230040	3861.10	17.87	15.01	19.53	1.32
Paine	PAR9MP	694568	4229850	5016.00	18.04	15.43	19.60	1.12
Paine	PAR6MP	694218	4229700	5563.29	18.39	14.86	20.32	1.52
Paine	PAR10MP	694068	4229730	5829.23	18.62	14.71	20.50	1.65
Paine	PARB2	693248	4230140	7055.48	18.60	14.54	20.57	1.67
Paine	PAR8MP	693137	4230180	7122.47	18.84	14.50	20.91	1.97
Piney	PIR1MP	736308	4292604	402.61	15.67	12.24	19.16	1.65
Piney	PIR3LCP	736218	4291980	1199.93	16.43	12.76	19.78	1.65
Piney	PIR4MP	735598	4291160	2480.47	16.55	13.24	19.65	1.51
Piney	PIR5MP	735458	4290050	3955.00	16.82	13.62	19.97	1.48
Piney	PIR6MP	736408	4289180	5862.79	17.74	15.87	20.49	1.15
Piney	PIR7MP	736748	4288300	7115.97	17.40	15.07	20.22	1.17
Piney	PIR8MP	737538	4287390	8756.79	17.88	14.63	20.55	1.39
Staunton	SR1MP	725248	4260810	477.07	14.64	11.96	17.33	1.32
Staunton	SR2MP	725908	4260450	1412.13	15.16	12.34	18.15	1.44
Staunton	SR5MP	726948	4259890	2907.57	15.92	13.03	19.08	1.51

Staunton	SR6MP	728018	4259921	4398.87	16.45	13.48	19.38	1.48
Staunton	SR10MP	728598	4259660	5220.08	17.12	13.88	19.84	1.48
Staunton	SR7MP	728718	4259390	5627.21	17.09	13.99	20.02	1.52
Staunton	SR9MP	729448	4258420	7519.72	17.41	14.57	19.88	1.33
White Oak	WOC1MP	728788	4273701	469.03	13.51	11.85	14.91	0.74
White Oak	WOC3MP	728998	4273160	1237.37	15.43	12.67	17.90	1.29
White Oak	WOC4MP	729268	4272400	2307.96	15.71	12.52	18.58	1.48
White Oak	WOC5MP	730288	4271180	4428.05	17.90	14.23	21.16	1.77
White Oak	WOC7LCP	730758	4270690	5302.94	18.69	15.02	22.07	1.79
White Oak	WOC8MP	730948	4269150	7356.87	18.29	15.88	19.78	1.07
White Oak	WOCB	731018	4269110	7448.09	18.71	16.04	21.18	1.28